AFAMRL-TR-84-006

TWO-DIMENSIONAL FAST FOURIER TRANSFORMS IN IMAGE PROCESSING

DONALD E. LEWIS, Ph.D.

SYSTEMS RESEARCH LABORATORIES, INC.
2800 INDIAN RIPPLE ROAD
DAYTON, OHIO 45440

JANUARY 1984

Approved for public release; distribution unlimited.

AIR FORCE AEROSPACE MEDICAL RESEARCH LABORATORY
AEROSPACE MEDICAL DIVISION
AIR FORCE SYSTEMS COMMAND
WRIGHT-PATTERSON AIR FORCE BASE, OHIO 45433

NOTICES

When US Government drawings, specifications, or other data are used for any purpose other than a definitely related Government procurement operation, the Government thereby incurs no responsibility nor any obligation whatsoever, and the fact that the Government may have formulated, furnished, or in any way supplied the said drawings, specifications, or other data, is not to be regarded by implication or otherwise, as in any manner licensing the holder or any other person or corporation, or conveying any rights or permission to manufacture, use, or sell any patented invention that may in any way be related thereto.

Please do not request copies of this report from Air Force Aerospace Medical Research Laboratory. Additional copies may be purchased from:

National Technical Information Service
5285 Port Royal Road
Springfield, Virginia 22161

Federal Government agencies and their contractors registered with Defense Technical Information Center should direct requests for copies of this report to:

Defense Technical Information Center
Cameron Station
Alexandria, Virginia 22314

TECHNICAL REVIEW AND APPROVAL

AFAMRL-TR-84-006

This report has been reviewed by the Office of Public Affairs (PA) and is releasable to the National Technical Information Service (NTIS). At NTIS, it will be available to the general public, including foreign nations.

This technical report has been reviewed and is approved for publication.

FOR THE COMMANDER

CHARLES BATES, JR.
Director, Human Engineering Division
Air Force Aerospace Medical Research Laboratory

Unclassified

SECURITY CLASSIFICATION OF THIS PAGE

REPORT DOCUMENTATION PAGE

1a. REPORT SECURITY CLASSIFICATION Unclassified	1b. RESTRICTIVE MARKINGS
2a. SECURITY CLASSIFICATION AUTHORITY	3. DISTRIBUTION/AVAILABILITY OF REPORT Approved for public release; distribution unlimited.
2b. DECLASSIFICATION/DOWNGRADING SCHEDULE	
4. PERFORMING ORGANIZATION REPORT NUMBER(S) AFAMRL-TR-84-006	5. MONITORING ORGANIZATION REPORT NUMBER(S)
6a. NAME OF PERFORMING ORGANIZATION Systems Research Laboratories, Inc. 6b. OFFICE SYMBOL (If applicable)	7a. NAME OF MONITORING ORGANIZATION Air Force Aerospace Medical Research Lab Human Engineering Division
6c. ADDRESS (City, State and ZIP Code) 2800 Indian Ripple Road Dayton, Ohio 45440	7b. ADDRESS (City, State and ZIP Code) AMD, AFSC, Wright-Patterson AFB Ohio 45433
8a. NAME OF FUNDING/SPONSORING ORGANIZATION 8b. OFFICE SYMBOL (If applicable)	9. PROCUREMENT INSTRUMENT IDENTIFICATION NUMBER F33615-82-C-0511
8c. ADDRESS (City, State and ZIP Code)	10. SOURCE OF FUNDING NOS. PROGRAM ELEMENT NO.: 62202F; PROJECT NO.: 7184; TASK NO.: 11; WORK UNIT NO.: 44
11. TITLE (Include Security Classification) TWO-DIMENSIONAL FAST FOURIER TRANSFORMS IN IMAGE PROCESSING	
12. PERSONAL AUTHOR(S) Donald F. Lewis, Ph.D.	
13a. TYPE OF REPORT Interim Technical 13b. TIME COVERED FROM 1982 TO 1983	14. DATE OF REPORT (Yr., Mo., Day) January 1984 15. PAGE COUNT 77
16. SUPPLEMENTARY NOTATION	

17. COSATI CODES			18. SUBJECT TERMS (Continue on reverse if necessary and identify by block number)
FIELD	GROUP	SUB. GR.	
05	05		Image Processing; Fourier Transform; Spatial Filtering; Displays
14	02		

19. ABSTRACT (Continue on reverse if necessary and identify by block number)

This report is intended to orient the reader to the application of the discrete two-dimensional (fast) Fourier transform in the context of digital image processing. Both mathematical and pictorial results (magnitude, phase, and power spectral density plots) are presented for a variety of rudimentary and more complex images. In addition, the VIPER (Visual Image Processing, Enhancement, and Reconstruction) digital image processing facility of the Air Force Aerospace Medical Research Laboratory is described.

20. DISTRIBUTION/AVAILABILITY OF ABSTRACT UNCLASSIFIED/UNLIMITED ☒ SAME AS RPT. ☐ DTIC USERS ☐	21. ABSTRACT SECURITY CLASSIFICATION Unclassified
22a. NAME OF RESPONSIBLE INDIVIDUAL Gilbert G. Kuperman	22b. TELEPHONE NUMBER (Include Area Code) 513-255-3727 22c. OFFICE SYMBOL AFAMRL/HEA

DD FORM 1473, 83 APR EDITION OF 1 JAN 73 IS OBSOLETE.

SECURITY CLASSIFICATION OF THIS PAGE

PREFACE

This report was initiated by the Air Force Aerospace Medical Research Laboratory, Wright-Patterson Air Froce Base, Ohio, to provide an introduction to the discrete, two-dimensional Fourier transform. The report was prepared by Systems Research Laboratories, Inc. (SRL), Dayton, Ohio 45440, under Contract F33615-82-C-0511. Mr. R. Bennett was the Air Force Contract Monitor, and Mr. G. Kuperman was the Air Force Manager for Work Unit 7184-11-44, "Image Display Mensuration/Enhancement."

The scope of the effort reported here has been such that the efforts of several people have been crucial to its conduct and successful completion. Each photographic data set shown involved a complicated set of operations, many of which were repeated several times in order to achieve the desired clarity. The author acknowledges with thanks the especially significant contributions of Mr. Gilbert G. Kuperman and 1st Lt. Donald Wallquist, both of AFAMRL, as well as Mr. David Robinow and Mr. Conrad Frye, both of SRL.

TABLE OF CONTENTS

LIST OF ILLUSTRATIONS

LIST OF ILLUSTRATIONS (continued)

LIST OF ILLUSTRATIONS (continued)

Section 1
INTRODUCTION

The application of linear systems theory, particularly in the context of digital image processing, has been demonstrated to provide powerful research approaches to a variety of problems in visual perception and human factors engineering of displays. It has supported methodologies in symbol legibility, display image quality assessment, reduction of aircraft observables, simulation of advanced cockpit display concepts, design of C^3I displays, and fundamental research into visual psychophysics. Digital image processing offers the researcher a means of generating highly controlled, calibrated visual stimuli in either hardcopy (photographic print or transparency) or softcopy (television) formats. Linear systems methods permit the researcher to exercise precise control over the spatial frequency content of an image.

The Human Engineering Division of the Air Force Aerospace Medical Research Laboratory (AFAMRL) has developed a state-of-the-art digital image processing facility to permit researchers in the laboratory, in other Air Force agencies, and at supporting university and industrial organizations to develop and apply digital image processing methods to current research issues. The Visual Image Processing, Enhancement, and Reconstruction (VIPER) facility continues to support the Optical Countermeasures and Deception, Radar Information Transfer Systems Analysis, C^3 Operator Performance Engineering, Strategic Avionics Crewsystem Development Engineering Facility, Windscreen Assessment, and Aviation Vision research and development programs within AFAMRL.

VIPER consists of an International Imaging Systems Model 70 image processing system hosted on a Digital Equipment Corporation PDP 11/45 equipped with dual disk and dual tape drives and operating under RSX-11M. Image quantization is performed using a digitizing tablet, a television camera, or an Eikonix Corporation digitizer. Hardcopy output is produced by either a Matrix Corporation or a Dicomed Corporation film recorder. Softcopy displays are presented on a variety (Tektronix, Conrac, SRL, Aydin) of color CRTs. A schematic outline of the facility and its capabilities is depicted in Figure 1.

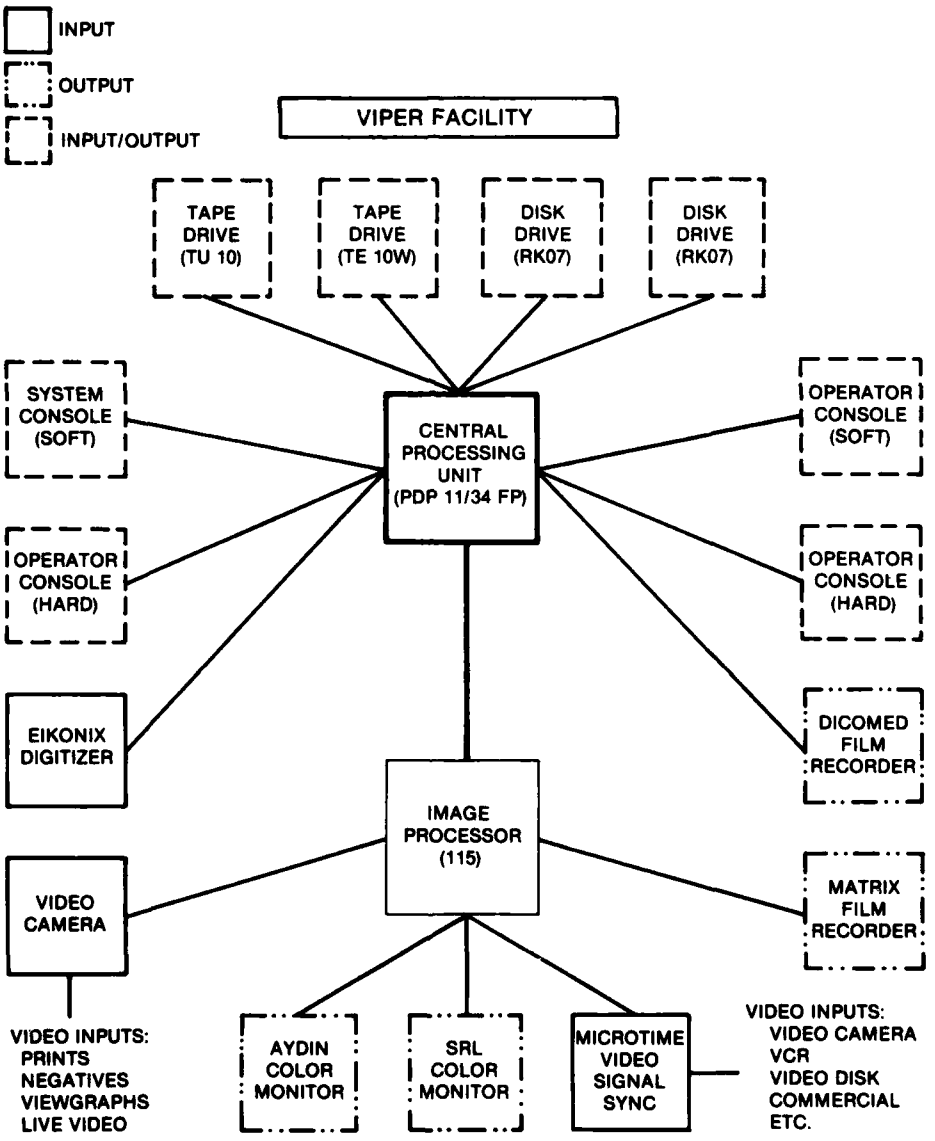

Figure 1. Schematic Outline of the VIPER Facility

Linear systems methods of spatial filtering are employed in VIPER to accomplish a variety of research objectives. Generally, these objectives are divided among three broad classes. Images are analyzed to determine various correlates of information content (i.e., image quality assessment). Images are spatially filtered so as to exhibit precise physical characteristics (i.e., stimulus generation). Images are reconstructed with specified physical characteristics emphasized (i.e., image enhancement).

In order to accomplish the specific research objectives at hand and to make effective use of a highly-interactive image processing capability such as VIPER, the investigator must be able to determine what processing should be performed and to evaluate how well a processed image satisfies his needs. An appreciation of Fourier transform-based image processing methods is clearly required of investigators in perception, sensor/display design, image quality evaluation, bioengineering, and the host of other disciplines that can exploit the power of Fourier analysis in designing and carrying out system simulations and operator performance studies.

The most logical approach to Fourier analysis is through a discussion of periodic functions. A periodic function of time is one that had its beginning in the infinite past, and will continue into the infinite future. Furthermore, a periodic function consists of a single pattern variation repeated endlessly over the function's doubly-infinite duration. This single pattern has the duration T, called the period of the function. An example function is portrayed in Figure 2. We note that T, the period, separates the starting times for the pulses (or the ending times, or the pulse centers, etc.). Any physical significance could be assigned to this function. For instance, the pulses could represent the time each day that the reader is at work; the absence of a pulse would then mean that the reader was otherwise occupied. This example (or any other) immediately discloses two problems with the definition of periodic temporal functions. They are:

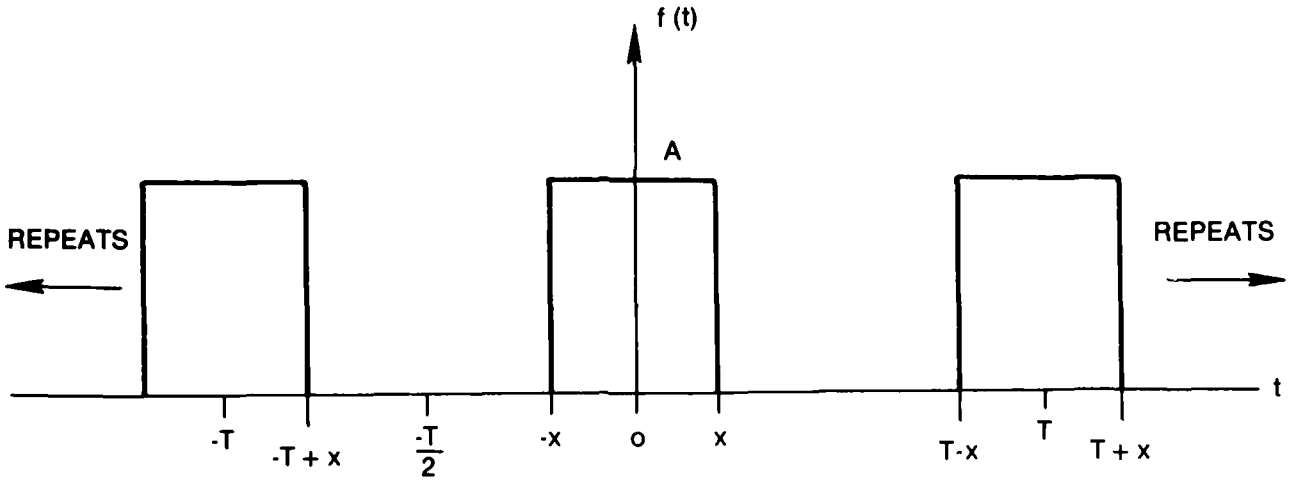

Figure 2. Example of a Periodic Function

1. A phenomenon must be under careful control to be such that each individual pattern (cycle) is exactly like every other one, in every respect.

2. No known phenomenon extends into the infinite past, or can be expected to extend into the infinite future.

The first problem can be handled by assuming that there is only one cycle or period of the functional variation, and that means are provided to have it occur repetitiously. The second problem, a philosophical one, can be dealt with by saying that if a large number of cycles of variation are allowed to occur (the phenomenon occurs over many periods), then the function can be successfully treated as if it were periodic. This treatment is not uncommon; inspection of a camera lens will disclose that the setting for infinite range is very close to that for 15 feet, and 15 feet is many times the focal length of the lens system. With this interpretation, Fourier analysis "works" very well.

It is postulated that any "periodic" temporal function, subject to the above constraints, may be represented as a linear combination of simpler periodic functions, having periods T_1, T_2, ..., T_n, where

$$T = nT_n,$$

or all but one ($n = 1$) of the functions have periods shorter than the period of the function under investigation. This linear combination is generally described as the infinite sum of a weighted set of basis functions, the set of basis functions being the set of "simpler periodic functions." An intuitively important set of basis functions is the sinusoids, or acoustically speaking, the "pure tones," since their combination with various weightings serves to assist us in classifying musical instruments (and artists) when a sustained ("periodic") sound is generated. From above, the case $n = 1$ is called the fundamental tone, and all larger values of n correspond to nth harmonics. This simple connection cannot be made for other sets of basis functions.

It is also true, one notes, that when a musical instrument produces other than a sustained sound, a dynamic combination of tones is produced, the description of which is more easily given in terms of the frequencies present (frequency = T^{-1}) than in terms of any temporal mathematical expression. Such a case is usually described mathematically in terms of frequency, but as a continuous function, rather than the discrete linear sum described for periodic functions. One is thus able to distinguish between passages played solo on a French horn, and the same passages played on an oboe, by virtue of the "spectral characteristics" (frequency content), even though the sounds produced are not sustained nearly long enough to be treated as periodic. Thus, while no single-frequency tone is present, one can intuitively accept the description in terms of frequency. This technique of analysis is commonly used, and is related to the use of the sinusoidal set of basis functions in periodic analysis.

Finally, two-dimensional phenomena of many types have descriptions in terms of frequencies, except that the frequencies are not measured per second (T^{-1}) but per unit of distance (λ^{-1}). These frequencies are termed "spatial frequencies." One thinks of venetian blinds; some have wide slats, some have narrow slats; the visual impressions obtained when looking through partially-open blinds can be quite different, or even pleasant or unpleasant. Some "light show" phenomena also demonstrate the effect. For important two-dimensional phenomena, analysis in terms of spatial frequencies is the only suitable approach, since the spatial details vary rapidly; one thinks of comparing the visual distribution on a television display to a musical passage. The source of psychophysical stimulation is the dynamic time-variation. Thus, for the television display, a meaningful mathematical analysis must be in terms of the spatial frequency content or capability.

The arguments given here in favor of analysis in terms of frequency content, temporal or spatial, are meant to be both intuitive and compelling; the technique is generally called Fourier analysis. The concepts, it has been argued, are quite simple; the analysis, it is admitted, can be cumbersome. The ideas given here are expressed mathematically in the following section, for the reader's convenience. The remainder of the material is presented in such a manner as to be useful without emphasis on mathematical descriptions.

Section 2
ANALYTIC BACKGROUND

Given a periodic time function, f(t) such that

$$f(t) = f(t \pm nT) \text{ for any integer } n \tag{1}$$

where T is the period of the function, the longest time interval over which the function does not replicate itself, as shown in Figure 1, then

$$f(t) = \frac{a_0}{2} + \sum_{n=1}^{\infty} [a_n \cos n\omega_0 t + b_n \sin n\omega_0 t] \tag{2}$$

where

$$\omega_0 = \frac{2\pi}{T} = 2\pi f \tag{3}$$

where f is the Hertzian frequency (cycles per second) and ω_0 the radian frequency (radians per second).

The coefficients may be evaluated from the given f(t) by:

$$\frac{a_0}{2} = \frac{1}{T} \int_{-\frac{T}{2}}^{\frac{T}{2}} f(t)\, dt = \text{average value of } f(t) \tag{4}$$

$$a_n = \frac{2}{T} \int_{-\frac{T}{2}}^{\frac{T}{2}} f(t) \cos n\omega_0 t\, dt \tag{5}$$

$$b_n = \frac{2}{T} \int_{-\frac{T}{2}}^{\frac{T}{2}} f(t) \sin n\omega_0 t\, dt \tag{6}$$

An alternate form is given by

$$f(t) = \sum_{n=-\infty}^{\infty} c_n \varepsilon^{jn\omega_0 t} \tag{7}$$

where

$$C_n = \frac{1}{T} \int_{-\frac{T}{2}}^{\frac{T}{2}} f(t)\, \varepsilon^{-jn\omega_0 t}\, dt \tag{8}$$

For functions of physical significance, it is assured that, for sufficiently large values of n, the coefficients a_n, b_n, and c_n are monotonically decreasing functions of n. Thus, if the tone produced by a baroque organ were taken as f(t), the components or "harmonics" close to the fundamental tone (n = 1) might be large (i.e., a_n and b_n, or c_n), but as n increases, the magnitude of each successive harmonic is lower than the last one, until finally inaudible to the human ear. One might observe that the harmonic content of the tones produced by an organ are much more convenient descriptors of the organ than an expression for f(t) to go with each tone.

As an example for reference, consider the periodic function of Figure 1:

$$f_p(t) = \begin{cases} A, & -x < t < x \\ 0, \text{ otherwise}, & -\frac{T}{2} < t < \frac{T}{2} \end{cases} \tag{9}$$

Thus,

$$a_n = \frac{2}{T} \int_{-\frac{T}{2}}^{\frac{T}{2}} f(t) \cos n\omega_0 t\, dt = \frac{2A}{T} \int_{-x}^{x} \cos n\omega_0 t\, dt$$

$$= \frac{2A}{n\omega_0 T} \sin n\omega_0 t \Big|_{-x}^{x} = \frac{4A}{n\omega_0 T} \sin n\omega_0 x$$

$$= \frac{4A}{} \left[\quad {}^{n\omega_0 x}_{} \right] \tag{10}$$

$$b_n = \frac{2}{T}\int_{-\frac{T}{2}}^{\frac{T}{2}} f(t)\ \sin n\omega_0 t\ dt = \frac{2A}{T}\int_{-x}^{x} \sin n\omega_0 t\ dt$$

$$= \frac{2A}{n\omega_0 T}\left[-\cos n\omega_0 t\right]_{-x}^{x} = 0 \tag{11}$$

$$c_n = \frac{1}{T}\int_{-\frac{T}{2}}^{\frac{T}{2}} f(t)\ \varepsilon^{-jn\omega_0 t}\ dt = \frac{A}{T}\int_{-x}^{x} \varepsilon^{-jn\omega_0 t}\ dt$$

$$= \frac{A}{-jn\omega_0 T}\varepsilon^{-jn\omega_0 t}\Big|_{-x}^{x} = \frac{2Ax}{T}\left[\frac{\sin n\omega_0 x}{n\omega_0 x}\right] \tag{12}$$

Here, the zero value for b_n is a consequence of symmetry, and the coefficient values (harmonic amplitudes) a_n and c_n depend on the function

$$\frac{a_n}{2} = c_n = \frac{2Ax}{T}\left[\frac{\sin n\omega_0 x}{n\omega_0 x}\right] \tag{13}$$

and

$$f(t) = \frac{2Ax}{T}\left[1 + 2\sum_{n=1}^{\infty}\left(\frac{\sin n\omega_0 x}{n\omega_0 x}\right)\cos n\omega_0 t\right] \tag{14}$$

$$= \frac{2Ax}{T}\sum_{n=-\infty}^{\infty}\left[\frac{\sin n\omega_0 x}{n\omega_0 x}\right]\varepsilon^{jn\omega_0 t} \tag{15}$$

Now, since

$$n\omega_0 x = n\pi\left(\frac{2x}{T}\right) \tag{16}$$

we see that the quantity $\left(\frac{2x}{T}\right)$, sometimes called the "duty cycle" for a rectangular pulse, determines the harmonic structure for the function.

A strategy of some utility is to plot the function c_n versus the variable ω. Since c_n is nonzero only for integer n, the plot is of a discrete

function, having nonzero values only at the harmonic frequencies, as shown in Figure 3. The plot of Figure 2 now depicts a "time-domain" description of $f_p(t)$, while Figure 3 depicts a "frequency domain" description.

In an analysis of a periodic function for serious purposes, obtaining an infinite-series representation is a step of questionable progress. Thus, it is usually concluded that all harmonics higher than the Nth (where N is usually selected, but sometimes calculated) are of negligible amplitude and are eliminated. The series is said to have been truncated, and the new function is said to be band-limited. That is, no harmonics are present outside the band of frequencies,

$$-N\omega_0 \leq \omega \leq N\omega_0$$

This simplification seems arbitrary, but is actually the source of only small errors in many physical problems. The concept of band-limited functions is very important in Fourier analysis.

Given these concepts related to periodic functions, it is a simple matter to conclude, in view of common experience, that nonperiodic functions of time have associated with them a description in terms of frequency. The human voice is an excellent example of this, in that spoken conversation is not periodic, but can be categorized by its frequency content (i.e., "male voice" versus "female voice," etc.). Furthermore, many important physical time functions that are not periodic are band-limited, as is the human voice, and can be treated as such, for instance in the design of telephone systems.

The mathematics of this situation are done using the Fourier transform,

$$F(j\omega) = \mathcal{F}[f(t)] = \int_{-\infty}^{\infty} f(t)\, \epsilon^{-j\omega t}\, dt \tag{17}$$

$$F(j\omega) = A\ (\omega)\ \epsilon^{j\theta(\omega)} \tag{18}$$

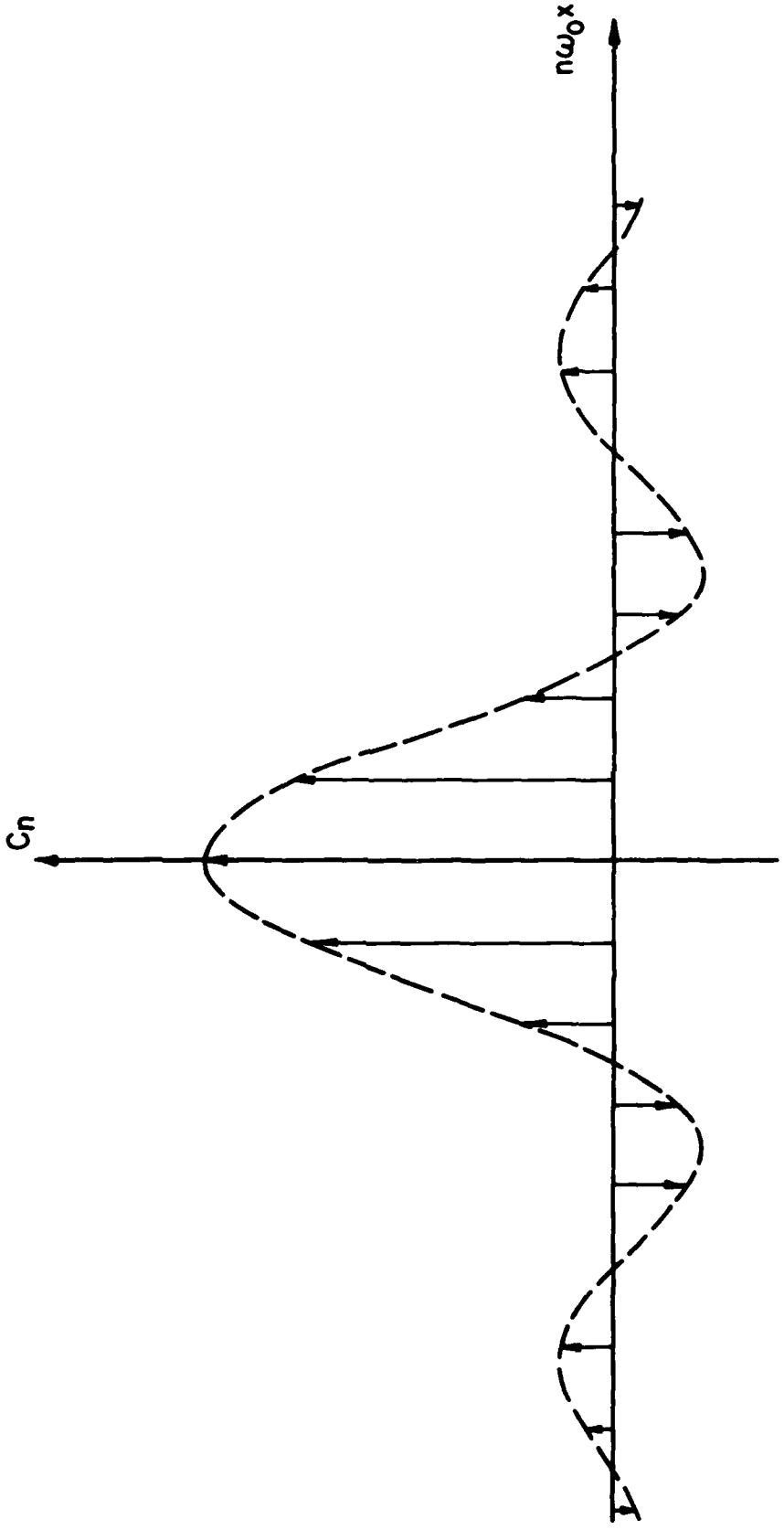

Figure 3. Plot of C_n Versus $n\omega_0 x$ for T = 10x

It should be noted here that the radian frequency, ω, is a continuous variable, as opposed to the discrete $n\omega_0$ encountered in the analysis of periodic functions.

As en example, let us define f(t) from Figure 2 such that

$$f(t) = \begin{cases} A, & -x \leq t \leq x \\ 0, & \text{otherwise, for } \underline{\text{all}} \text{ time} \end{cases} \tag{19}$$

Thus, this function is not periodic, but consists of a single rectangular pulse. Now,

$$\begin{aligned} F(j\omega) &= \int_{-\infty}^{\infty} f(t)\ \varepsilon^{-j\omega t}\ dt = A \int_{-x}^{x} \varepsilon^{-j\omega t}\ dt \\ &= \frac{A}{-j\omega}\ \varepsilon^{-j\omega t}\ \Big|_{-x}^{x} = \frac{2A}{\omega} \sin \omega x \\ &= 2Ax \left[\frac{\sin \omega x}{\omega x}\right] \end{aligned} \tag{20}$$

The similarity to Equation (12) is obvious; Equation (20) is depicted by the "envelope function" of Figure 3, with normalized T.

The calculation of $F(j\omega)$ for typical mathematical functions is often easily accomplished. Similarly, operations in the time domain can be shown to have equivalent (and, in many important cases, simpler) operations in the frequency domain.

Two-dimensional functions or spatial functions exist which are not time-varying, but which can be described in terms of their spatial extent, especially in terms of their extent within the field-of-view (FOV) of an instrument, or observer. For instance, if this printed sheet of paper is viewed by a human observer in an otherwise-black FOV, then:

1. If only one letter falls in focus within the FOV, it is easily recognized, and corresponds to a low spatial frequency phenomenon (i.e., not a lot is happening per unit angle in the FOV).

2. If only one word falls in focus within the FOV, it is also easily recognized, and corresponds to a higher spatial frequency containing more information.

3. As the viewer distance increases, the entire page can be read, then only black lines on the white page are discernible, then the page appears as a white rectangle, a "dot," and finally nothing.

Thus, our sight/perception mechanism is determined by spatial frequencies, as our hearing/perception mechanism is determined by temporal frequencies. We are surrounded by physical temporal/hearable phenomena that we cannot hear because of the band-limited response of our ears. We are surrounded by physical spatial/seeable phenomena that we cannot see, because of the band-limited response of our eyes. Changes in our position relative to the phenomena may or may not change the situation. It would seem to be appropriate to apply the ideas of Fourier analysis in the two-dimensional case involving linear processes, because of the historical successes obtained with that technique. Thus, the two-dimensional Fourier transform is defined:

$$\mathcal{F}[f(x,y)] = F\ (j\omega_1,\ j\omega_2) = \int_{-\infty}^{\infty}\int_{-\infty}^{\infty} f(x,y)\ \varepsilon^{-j\omega_1 x}\ \varepsilon^{-j\omega_2 y}\ dxdy \tag{21}$$

$$= A\ (\omega_1,\ \omega_2)\ \varepsilon^{j\theta(\omega_1)}\ e^{j\phi(\omega_2)} \tag{22}$$

where

ω_1 is the spatial frequency associated with variations in the x-direction, and

ω_2 is the spatial frequency associated with variations in the y-direction.

For instance, we may consider a single white letter A formed in a 5 x 7 format in an otherwise black FOV, depicted in Figure 4.

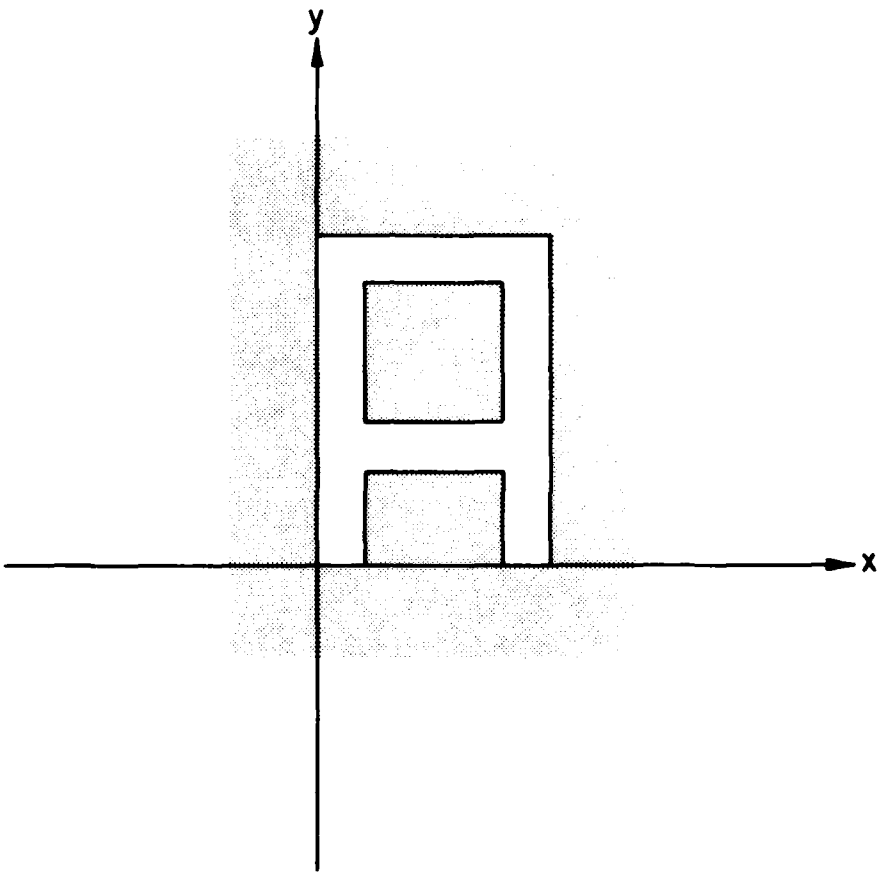

Figure 4. Block Letter in a 5 x 7 Format

In the x-direction, there are two lines per five spatial units, while in the y-direction, there are two lines per seven spatial units. Thus, lower fundamental spatial frequencies are associated with the longer dimension of the figure, and higher fundamental spatial frequencies are associated with the shorter dimension of the figure.

At this point, we may list characteristics of the transform of Equations (21) and (22) which are necessary for general utility.

1. $\mathcal{F}[Kf(x,y)] = k\,[\mathcal{F}f(x,y)]$ (23)

   Thus, only the relative brightness or density should be involved in determining the transform characteristics. The absolute brightness or density represents merely a multiplicative constant.

2. The transform should possess characteristics that are invariant under translation in the FOV.

3. The transform should possess characteristics that are invariant under rotation in the FOV.

The transform given possess all these characteristics and more, as will be shown.

As an example, consider a rectangular solid of height A and base 2b x 2b, situated with the base centered in the x-y plane. Then

$$\mathcal{F}[f(x,y)] = F(j\omega_1, j\omega_2) = \int_{-b}^{b}\int_{-b}^{b} A\,\varepsilon^{-j\omega_1 x}\,\varepsilon^{-j\omega_2 y}\,dxdy \tag{24}$$

$$= \frac{A}{(-j\omega_1)(-j\omega_2)}\,\varepsilon^{-j\omega_1 x}\Big|_{-b}^{b}\,\varepsilon^{-j\omega_2 y}\Big|_{-b}^{b} \tag{25}$$

$$= \frac{4A}{\omega_1\omega_2}\sin\omega_1 b\,\sin\omega_2 b \tag{26}$$

$$= 4Ab^2\left[\frac{\sin\omega_1 b}{\omega_1 b}\right]\left[\frac{\sin\omega_2 b}{\omega_2 b}\right] \tag{27}$$

One notes that $4Ab^2$ is the volume of the solid, and that the remainder of the expression is the same as we have associated with rectangular temporal pulses, except that it is also two-dimensional. There is, thus, a thread of unity established among the various functional renditions to which Fourier analysis is applied.

Finally, it must be noted that the Fourier analysis described above does not lend itself to machine (i.e., digital computer) implementation because of the implied continuity of the functions, and of the Lebesgue integrals. To circumvent this difficulty, another function has been defined--the discrete Fourier transform (DFT). In the use of this transform, the function of time, f(t), or of position, f(x,y), is assumed to be "sampled" or evaluated only at discrete points over its domain. The transform operation, which is generally done by a computer or specialized processor, then produces another set of discrete points in the appropriately-dimensioned frequency domain which generally approximates samples of the Fourier transform of the original continuous function. The "goodness" of the approximation depends on many things, but largely on the number of samples of the original function that are obtained. As the number of samples increases, the approximation improves; the calculation time also increases, of course, along with the requirement for machine memory.

To alleviate these problems, the fast Fourier transform (FFT) is generally the one that is machine-implemented; it is merely an algorithm for computation of the DFT using special techniques to reduce the time (in the machine) required for the calculation. An explanation of these transforms is beyond the intended scope of this document.

Section 3
THE VIPER CAPABILITY

The Visual Image Processing, Enhancement, and Reconstruction (VIPER) laboratory facility includes an I^2S Model 70E and DEC PDP 11/45 combination, with outstanding capabilities for digital image processing. With this equipment grouping, it is possible to display a visual image on a CRT, obtained from:

- a video camera
- a video tape
- computer storage, or
- computer generation

and modify the image to suit the purposes of the experimenter. The apparatus is capable of then doing a two-dimensional FFT of the image, providing the output information points as real part and imaginary part, or magnitude and phase. A map of the output (real part, imaginary part, magnitude, or phase) one parameter at a time, full screen can be displayed, and reproduced immediately on Polaroid© prints, or, with processing delays, in a number of other formats, including pseudocolor--enhanced images! That is, the input image is presented in the x-y plane on a CRT display. After two-dimensional transformation, two quantities correspond unambiguously to each single original point. In a planar, or two-dimensional display, these derived quantities can be presented, full screen, only one at a time. By using split-screen techniques, however, the parameters can be displayed simultaneously. The input image must be static, because the time required for the transformation is not negligible. Dynamic transformation of a running video tape, for instance, is not possible.

Several definitions must be made in preparation for two-dimensional fast Fourier transform (2DFFT) processing. They are:

1. The field-of-view size, in pixels.

2. The image size, in pixels. (It is frequently convenient not to fill the entire field-of-view with image of interest for 2DFFT processing, as some of the higher spatial frequencies may be lost.)

3. The relationship between image brightness and the quantity that it represents (object height, strength, etc.).

4. Any effects that might be produced because the image pixels do not occur at uniform spacing.

5. All the same parameters must be accounted for in the output images.

It should be noted that, while the pictorial output transformation is extremely informative and convenient for purposes of interpretation, the video and photographic processes may contain uncontrolled variables, which can give rise to phenomena for which there is no accounting. Thus, if accurate <u>data</u> on a transformation is required, a numerical printout is available from the system, and should be used. In this process, one truly becomes familiar with the staggering volume of data generated, and the difficulty involved in interpretation. Thus, one may use the pictorial version to isolate those areas requiring additional study, to reduce the size of printout that must be actually analyzed.

For a simple example, an approximation to the unit-impulse function is selected. The approximation consists of one white pixel in an otherwise-black surround of 128 x 128 pixels. This function is defined as

$$\delta (x - x_0, y - y_0), \text{ where}$$

$$\delta (x - x_0, y - y_0) = 0 \text{ for } x \neq x_0 \text{ and } y \neq y_0$$

and

$$\int_{x_0-\varepsilon}^{x_0+\varepsilon} \int_{y_0-\varepsilon}^{y_0+\varepsilon} \delta\,(x - x_0, y - y_0)\, dxdy = 1$$

The unit impulse function is, thus, defined as a function of infinitesimal width, infinite magnitude, and unity volume. It may be compared to an ideal point source, for instance, using the definition,

$$F\,(j\omega_1, j\omega_2) = \int_{-\infty}^{\infty} \int_{-\infty}^{\infty} \delta\,(x - x_0, y - y_0)\, \varepsilon^{-j\omega_1 x}\, \varepsilon^{-j\omega_2 y}\, dxdy \tag{28}$$

$$= [1]\, \varepsilon^{-j\omega_1 x_0}\, \varepsilon^{-j\omega_2 y_0} \tag{29}$$

The 2DFTT has been performed for several values of x_0, all with $y_0 = 0$.

The remaining figures consist of four photographs each of which, when taken as a whole, is called a "Pictorial Transform Study" of the image named in the title. All photographs within a figure have been made with the same scale factor, as measured in pixels. In each figure, the upper left frame is a photograph of a computer-generated rendition of the image under study. The upper right frame is a photograph of the magnitude of the 2DFFT of the image under study. The lower left frame is a photograph of the phase of the 2DFFT of the image under study. The lower right frame is a photograph of the power spectral density (PSD) of the image under study, with the (0,0) value arbitrarily set equal to zero. This value represents the average brightness of the image within the FOV, and will ordinarily be large in comparison with other values in the domain since no negative brightness values are permitted. Most images would, therefore, appear to have all the power associated with them concentrated at "D.C." The information sought is at other points in the distribution. The "Pictorial Transform Study" set of photographs, thus, contains the maximum amount of information that can be associated with the image under study by the methods being employed here. For $x_0 = 0$, $y_0 = 0$,

$$F\,(j\omega_1, j\omega_2) = 1 \tag{30}$$

as shown in Figure 5. Here, and in all that follows, the upper left photo is a "picture" of the image to be processed. Clearly, there is a single white pixel at the center of this frame, which corresponds to $\delta(x,y)$, the case in which $x_0 = y_0 = 0$. The upper right frame is the magnitude of modulus of $F(j\omega_1, j\omega_2)$ written upper right frame =

$$|F(j\omega_1, j\omega_2)| = A(\omega_1, \omega_2) \tag{31}$$

$$\text{Lower right frame} = \theta(\omega_1) + \phi(\omega_2) \tag{32}$$

where the notation is taken from Equations (21) and (22). Thus, in Figure 5, the impulse is shown in the upper left frame. The magnitude (1) is shown in the upper right frame, in which the assignment has been made white = 1, black = 0. Any irregularities or variations that are detected have entered during film processing, or during printing. The lower left frame depicts the phase which is in this case zero, and the assignment 0° = gray has been made. The lower right frame depicts the power spectral density (PDS), which is the square of the magnitude of $F(j\omega_1, j\omega_2)$, with the value at $\omega_1 = 0$, $\omega_2 = 0$ set equal to zero, since this value is frequently large enough to "swamp out" the other values.

In Figure 6, $x_0 = 4$ pixels, $y_0 = 0$. In the upper left frame, the single white pixel can be seen to be in the center vertically, but slightly displaced to the right horizontally, when compared to Figure 5. As previously discussed, $A(\omega_1, \omega_2)$ is exactly the same as in Figure 5, as is the PSD, of course. However, the phase now shows a strong variation, where the range has been set as follows:

$\theta(\omega_1) = -180° = -\pi$ rad. → black

$\theta(\omega_1) = 0° = 0$ rad. → gray

$\theta(\omega_1) = 180° = \pi$ rad. → white

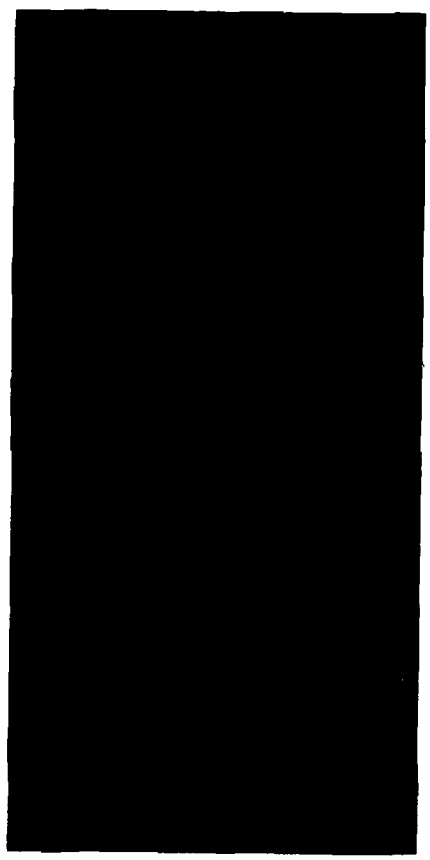

Figure 5. Pictorial Transform Study of a Unit Impulse or "Delta Function" Located at (0,0)

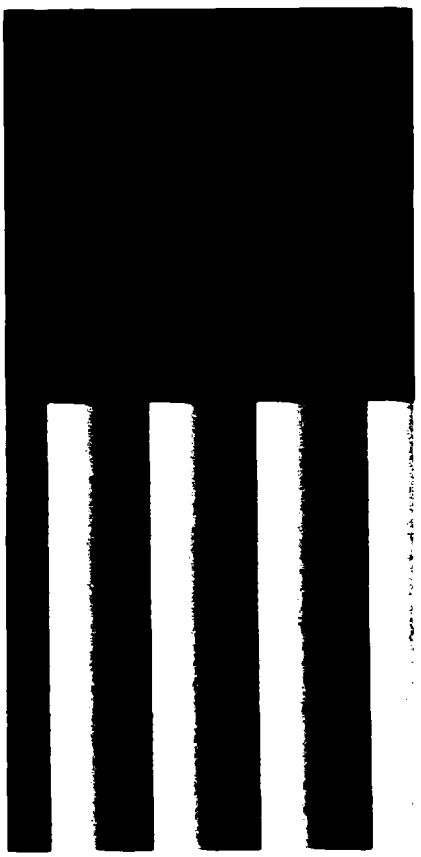

Figure 6. Pictorial Transform Study of a Unit Impulse or "Delta Function" Located at (4,0)

Thus,

$$F(j\omega_1, j\omega_2) = 1\ \varepsilon^{-j\omega_1, x_0} \tag{33}$$

where $x_0 = 4$ pixels.

In Figure 7, $x_0 = 28$ pixels, $y_0 = 0$. Again, the transform magnitude and PSD remain the same, while the phase undergoes another drastic change in nature.

Finally, in Figure 8, $x_0 = 60$ pixels, $y_0 = 0$, and the same phenomena are noted.

From the above, one might be tempted to generalize as follows:

$$F(j\omega_1, j\omega_2) = K\,[A(\omega_1, \omega_2)]\ \varepsilon^{j\theta(\omega_1)}\ \varepsilon^{j\phi(\omega_2)} \tag{34}$$

where:

K tells us "how much" exists.

$A(\omega_1, \omega_2)$ tells us what the shape is, and

$\theta(\omega_1) + \phi(\omega_2)$ tells us "where" the shape is within the FOV.

This generalization can be used carefully, with the knowledge that it is incorrect, since $A(\omega_1, \omega_2)$, $\theta(\omega_1)$, and $\phi(\omega_2)$ are not independent functions, but depend, one on the others in a complicated relationship.

In Figures 5, 6, 7, and 8, no variation in $\phi(\omega_2)$ is present. That is because $y_0 = 0$ in all cases. In general, both $A(\omega_1, \omega_2)$ and $\theta(\omega_1)$, $\phi(\omega_2)$ vary throughout the $\omega_1 - \omega_2$ plane. A good example of this variation is provided by the calculations in Equations (24) through (27) for a rectangular solid situated with its base centered in the x-y plane. Figure 9 depicts the results of that calculation for a base size of 35 x 35 pixels (b = 17 pixels) and a height, or brightness of A. The calculated result was

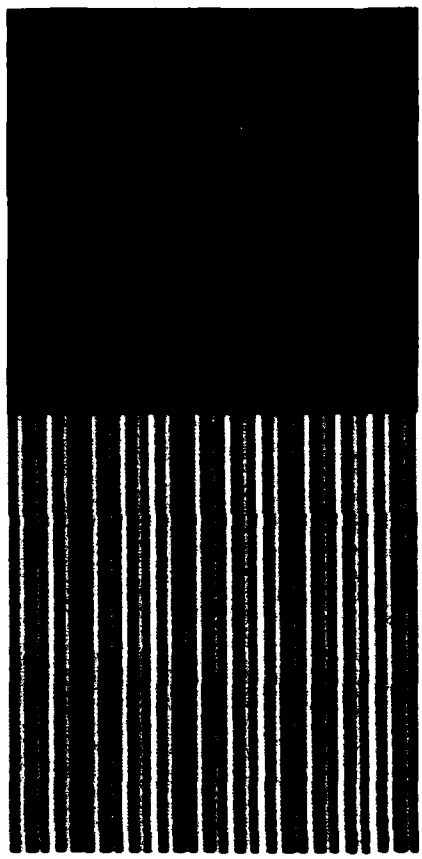

Figure 7. Pictorial Transform Study of a Unit Impulse or "Delta Function" Located at (28,0)

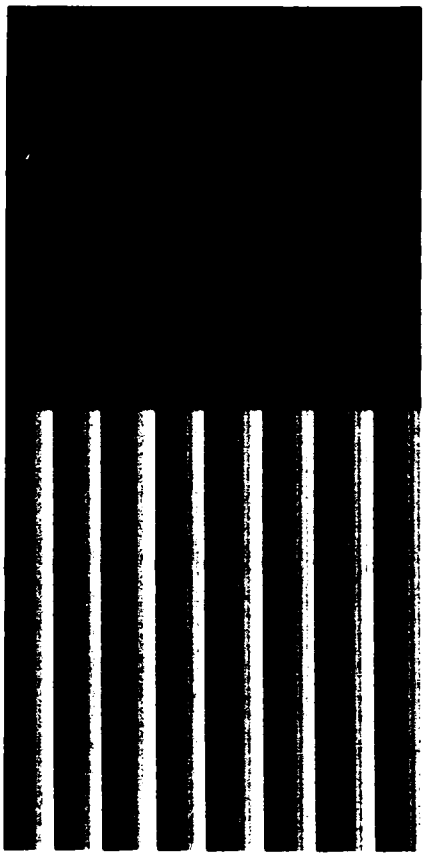

Figure 8. Pictorial Transform Study of a Unit Impulse or "Delta Function" Located at (60,0)

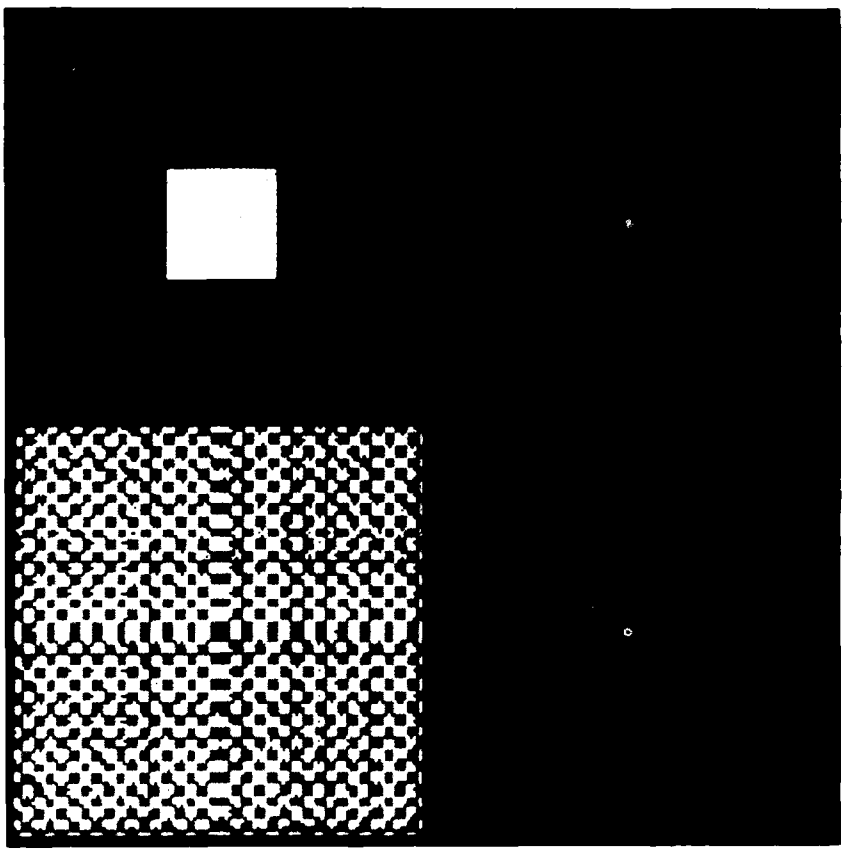

Figure 9. Pictorial Transform Study of a Square
35 x 35 Pixels, Centered at (0,0)

$$F(j\omega_1, j\omega_2) = 4Ab^2 \left[\frac{\sin \omega_1 b}{\omega_1 b}\right]\left[\frac{\sin \omega_2 b}{\omega_2 b}\right] \tag{35}$$

Here, $K = 4Ab^2$ has been scaled for the machine, and is not directly retrievable. However,

$$A(\omega_1, \omega_2) = \left[\frac{\sin \omega_1 b}{\omega_1 b}\right]\left[\frac{\sin \omega_2 b}{\omega_2 b}\right] \tag{36}$$

is very clearly shown, especially along the ω_1 - ω_2 axes. The off-axis components have been attenuated by the photographic procedures. However,

$$\text{Phase} = \theta(\omega_1) + \phi(\omega_2) = 0 \rightarrow \text{gray or } \pi \rightarrow \text{white}$$

is very well depicted for all of the ω_1 - ω_2 plane contained in the frame. This pheonmenon will be noted for most figures of any complexity; that is, the phase information will be retained photographically with much better fidelity than the magnitude information.

In Figure 10, the same square has been displaced by 17 pixels in the +y direction (i.e., $x_0 = 0$, $y_0 = 17$ pixels). The magnitude remains unchanged, the phase variation in the ω_1 (corresponding to x) direction remains unchanged, but a linear phase variation in the ω_2 (corresponding to y) direction is evident. The corresponding transform expression is

$$F(j\omega_1, j\omega_2) = 4Ab^2\, \varepsilon^{-j\frac{\omega_2 y_0}{2}} \left[\frac{\sin \omega_1 b}{\omega_1 b}\right]\left[\frac{\sin \omega_2 b}{\omega_2 b}\right] \tag{37}$$

In Figure 11, the same square has been displaced by 17 pixels in the +x direction (i.e., $x_0 = 17$ pixels, $y_0 = 0$). Again, the magnitude function is unchanged, as is the ω_2 phase variation (from Figure 9); however, a linear phase variation in the ω_1 (corresponding to x) direction is evident. The corresponding transform expression is

$$F(j\omega_1, j\omega_2) = 4Ab^2\, \varepsilon^{-j\frac{\omega_1 x_0}{2}} \left[\frac{\sin \omega_1 b}{\omega_1 b}\right]\left[\frac{\sin \omega_2 b}{\omega_2 b}\right] \tag{38}$$

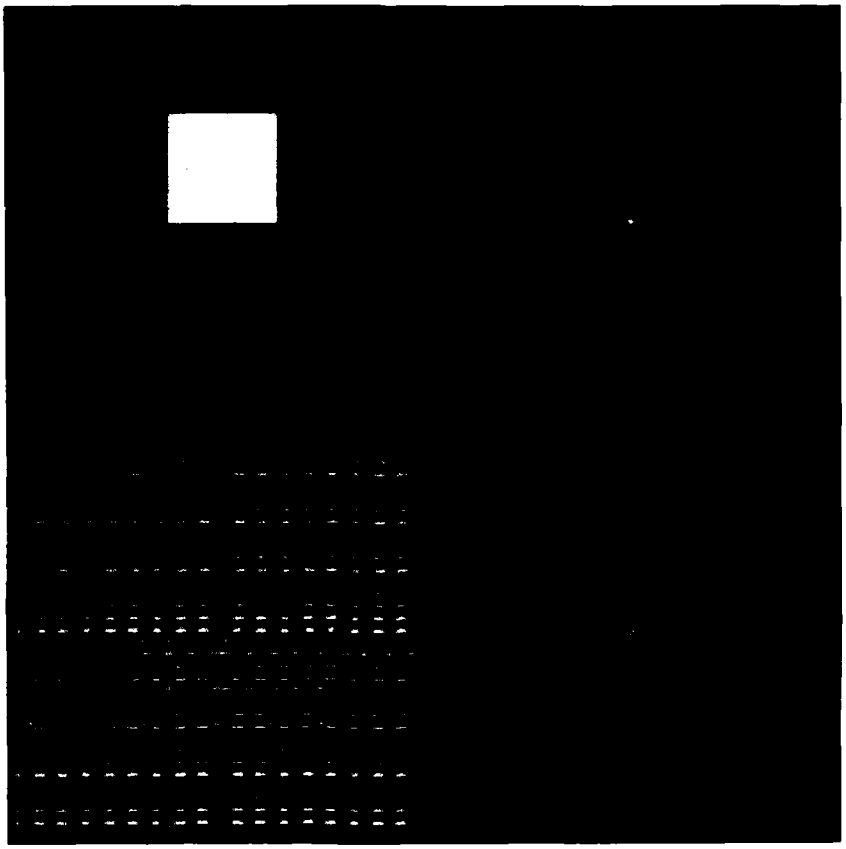

Figure 10. Pictorial Transform Study of a Square 35 x 35 Pixels, Centered at (0,17)

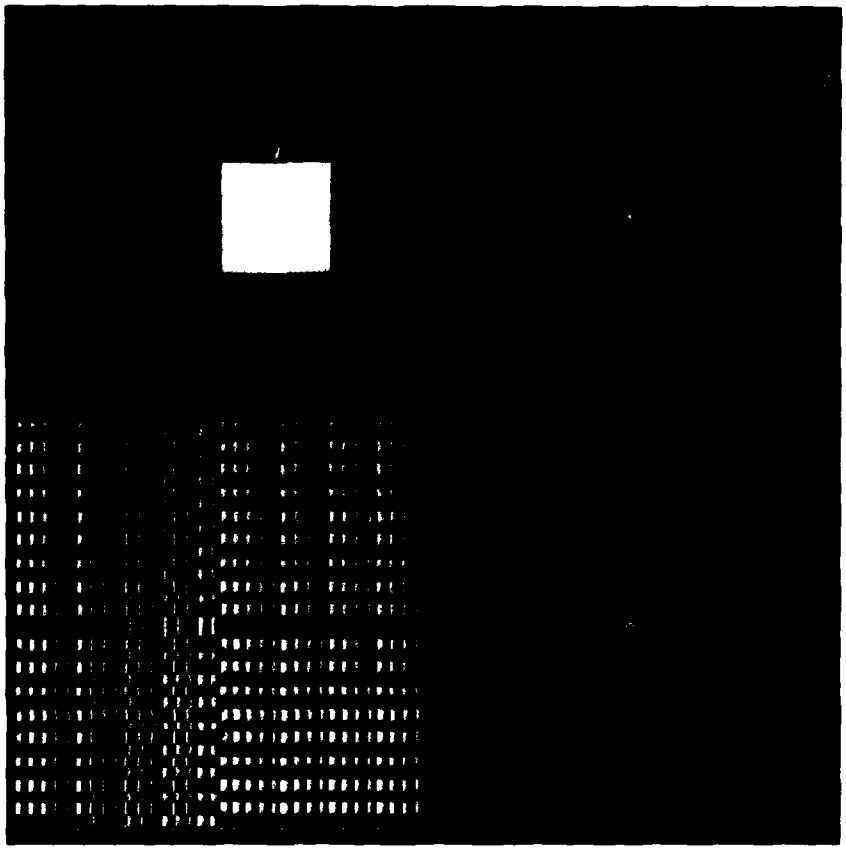

Figure 11. Pictorial Transform Study of a Square
35 x 35 Pixels, Centered at (17,0)

Finally, in Figure 12, $x_0 = y_0 = 17$ pixels, and the phase variation appears to be extremely complicated, while the remaining variables exhibit familiar properties. The corresponding transform expression is

$$F(j\omega_1, j\omega_2) = 4Ab^2 \, \varepsilon^{-j\frac{\omega_1 x_0}{2}} \, \varepsilon^{-j\frac{\omega_2 y_0}{2}} \left[\frac{\sin \omega_1 b}{\omega_1 b}\right]\left[\frac{\sin \omega_2 b}{\omega_2 b}\right] \qquad (39)$$

The transform is invariant under translation, only in its magnitude. Phase variation under translation may be described as strong.

Rotation of the square is depicted in Figure 13a, the angle of rotation, 45 degrees, not being to a symmetry axis of the display pixels. For that reason, the square edges are not smooth, and some size scaling was required. While the square is still approximately the same size within the FOV, each side of the square is 25 pixels, rather than 35. The square is centered in the x-y plane. The magnitude information appears to have been rotated, also by 45 degrees. The phase information, however, is not the same as that of Figure 8 rotated by 45 degrees, although on lines corresponding to the rotated $\omega_1 - \omega_2$ coordinate system, the approximation to simple rotation is good. It can, thus, be concluded that image orientation within the x-y place is extremely important, especially when the field-of-view is held constant. One might anticipate that a similarly rotated square in a 256 x 256 pixel surround would, by virtue of superior sample spacing, produce results more like those desired, as depicted in Figure 13 (this represents a small increase in performance for a substantial increase in computation size).

An excellent image for further investigation of this problem is the circle, itself insensitive to rotation, and also not capable of faithful rendition in a field of 128 x 128 pixels, as depicted in Figure 14. The transform of this figure should be a bright circular disk in the center, surrounded by alternating rings, as shown in the magnitude plot. The phase plot should be similar, with alternating gray (phase = 0) and white (phase = π) rings, each of the same radial thickness, and of smooth circular shape. Inspection of the phase frame shows that the rings are never smoothly circular and, as one

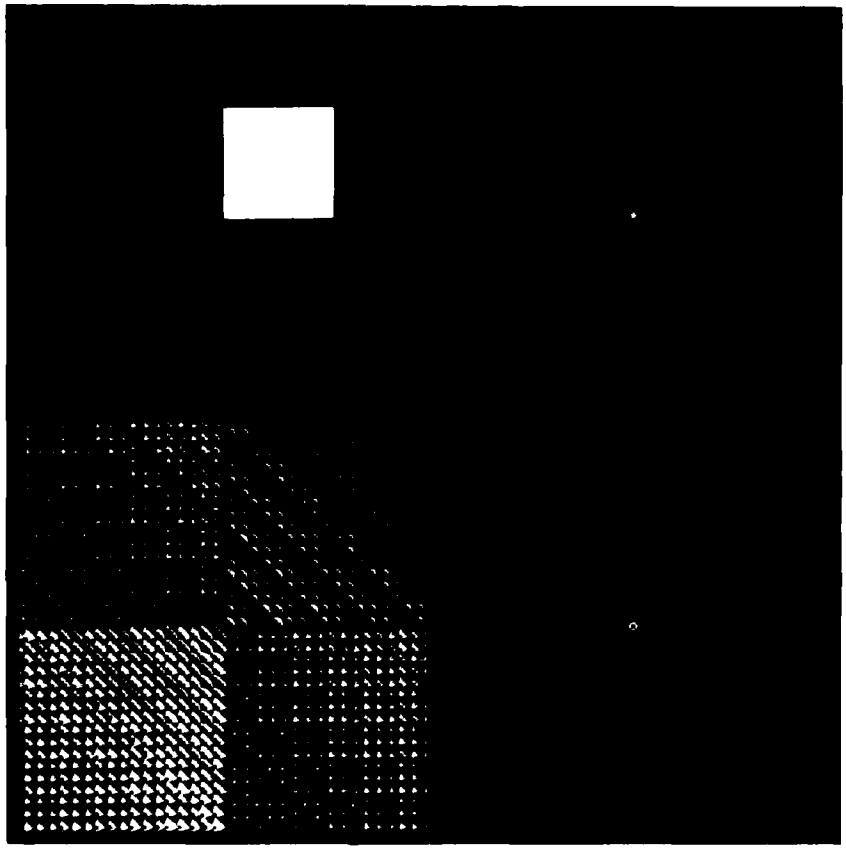

Figure 12. Pictorial Transform Study of a Square
35 x 35 Pixels, Centered at (17,17)

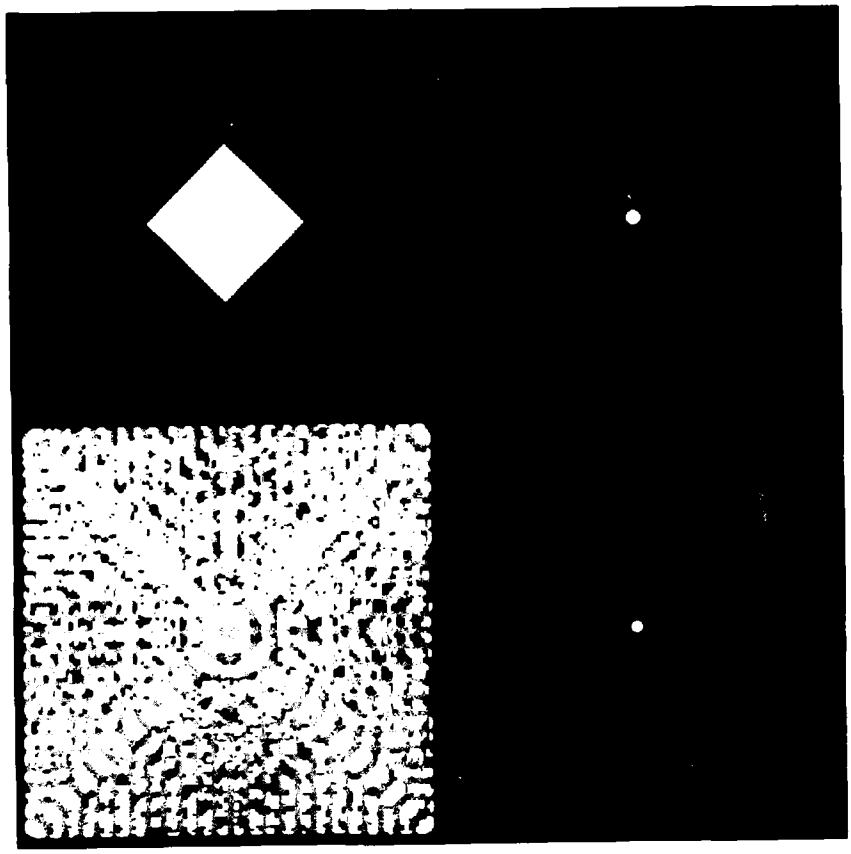

Figure 13a. Pictorial Transform Study of a Square 25 x 25 Pixels, Centered at (0,0), and Rotated by 45 Degrees

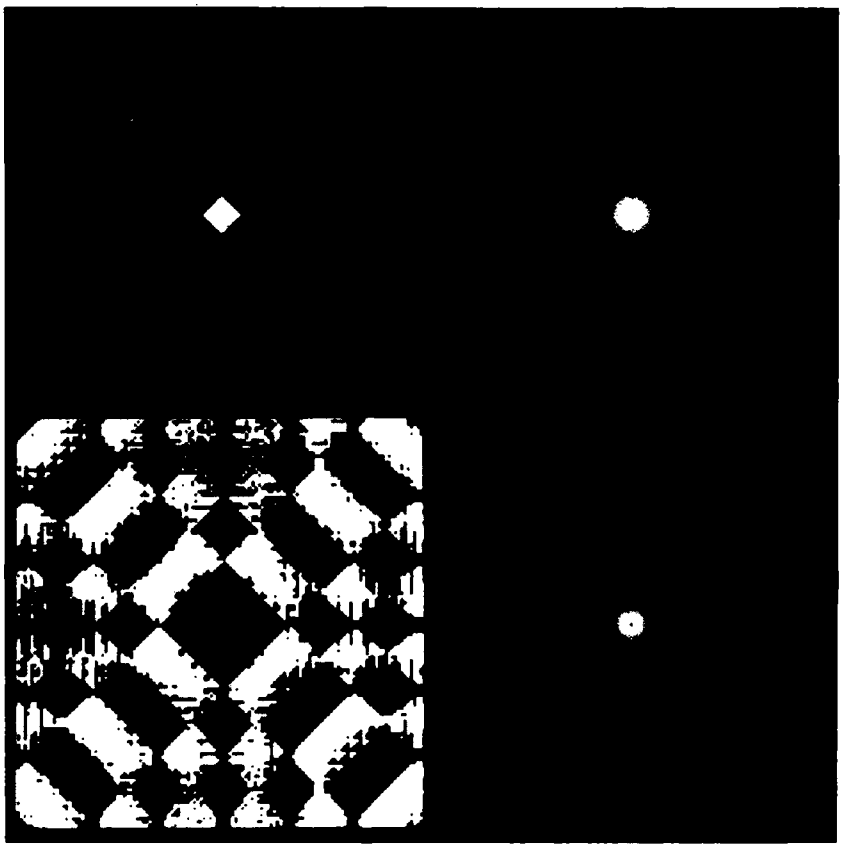

Figure 13b. Pictorial Transform Study of a Square 25 x 25 Pixels, Centered at (0,0), and Rotated by 45 Degrees, and in a 256 x 256 Pixel Field

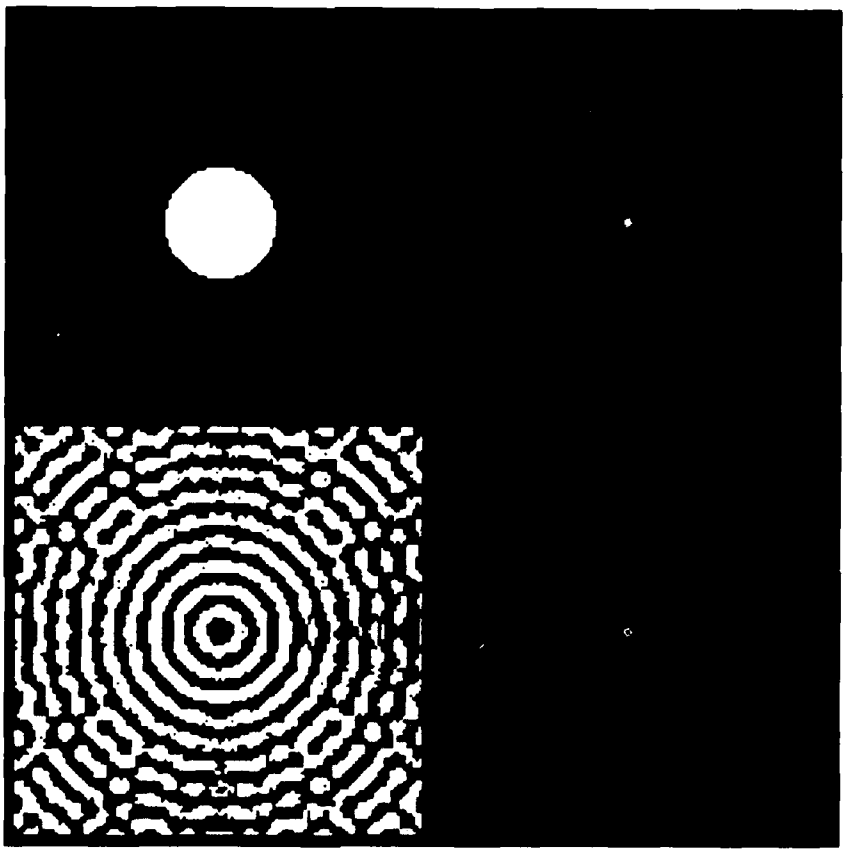

Figure 14. Pictorial Transform Study of a 35 Pixel-Diameter Circle, Centered at (0,0)

progresses outward from the center, the "rings" cease to be true rings, but begin to show a structure, indicating that the original image is not truly circular. Here, the frequency corresponding to radius in a $\omega - \phi$ plane, the transform is a Bessel function, as in the optical Airy disk:

$$F(j\omega) = \sqrt{2}\,\frac{J_1(\omega)}{\omega} \tag{40}$$

In this section, the analytic background of 2DFFT image processing has been introduced, and the evaluation of gross transform properties has been used to confirm the general correctness of the results obtained. However, certain limitations that may be imposed by the field-of-view in which the image is observed have been disclosed, to place the esrtwhile experimenter on guard when formulating the imagery to be processed.

Section 4
PICTORIAL TRANSFORM ANALYSIS

The VIPER photographic output consists of point data that are obscured by film characteristics and processing. The system includes provisions for "blowing up" the pictorial output so that each original pixel of data occupies several pixels in a square array. However, in using this process, higher frequency components are "lost" (i.e., not present on the photograph if the output array is held to the size of the input array), so that this technique also has its disadvantages.

For purposes of clarification, consider a rectangular image 35 pixels high and 7 pixels wide, centered in a 128 x 128 pixel field-of-view, as shown in Figure 15. The 5:1 aspect ratio in the image should be preserved in the transform.

Analytically,

$$F(j\omega_1, j\omega_2) = \int_{-17}^{17} \left[\int_{-3}^{3} f(x,y)\, \varepsilon^{-j\omega_1 x}\, dx \right] \varepsilon^{-j\omega_2 y}\, dy \qquad (41)$$

where f(x,y) has been normalized to unity within the rectangle, and zero outside.

Calculating,

$$F(j\omega_1, j\omega_2) = \int_{-17}^{17} \left[\frac{1}{-j\omega_1} \varepsilon^{-j\omega_1 x} \right]_{-3}^{3} \varepsilon^{-j\omega_2 y}\, dy \qquad (42)$$

$$= \int_{-17}^{17} \left[\frac{2}{\omega_1} \sin 3\omega_1 \right] \varepsilon^{-j\omega_2 y}\, dy \qquad (43)$$

$$= \frac{4}{\omega_1 \omega_2} \sin 3\omega_1 \sin 17\omega_2 \qquad (44)$$

$$= 204 \left[\frac{\sin 3\omega_1}{3\omega_1} \right] \left[\frac{\sin 17\omega_2}{17\omega_2} \right] \qquad (45)$$

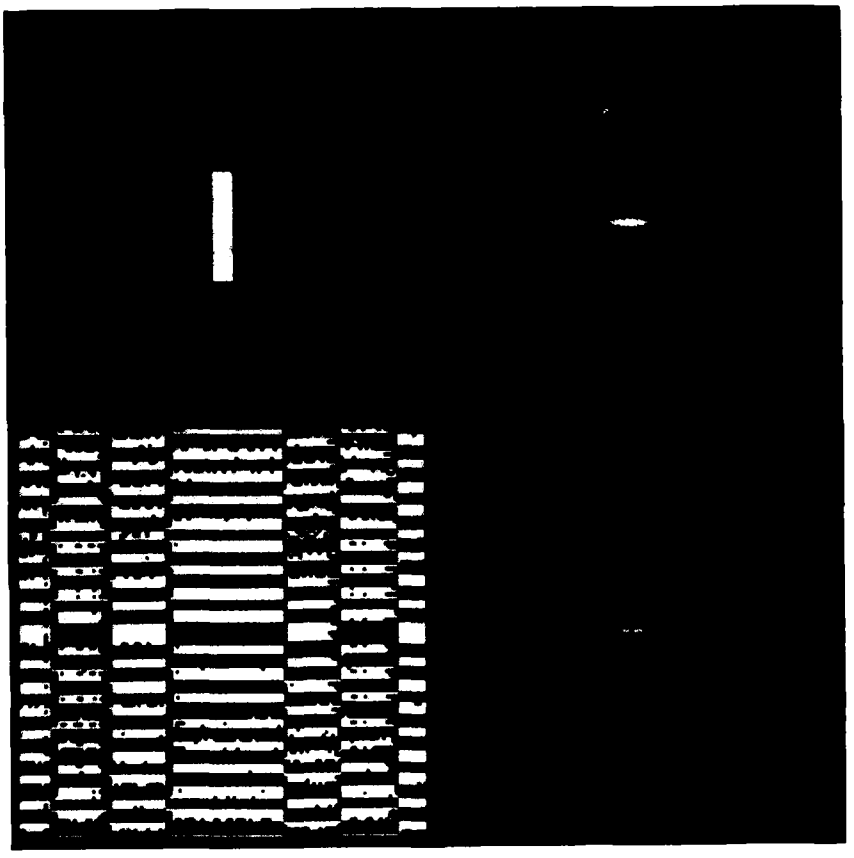

Figure 15. Pictorial Transform Study of a Rectangle, 7 x 35 Pixels, Centered at (0,0)

Inspection of the magnitude in Figure 15 discloses the presence of two normal sinc functions. However, brightness falls off rapidly on the axes, and the off-axis components are essentially undetectable. The phase "plot" of Figure 15 is, however, relatively unambiguous. By counting phase changes from the center of the center (largest) phase area, one finds that

$$-\frac{7\pi}{2} < 3\omega_1 < \frac{7\pi}{2}$$
$$-\frac{35\pi}{2} < 17\omega_2 < 17\pi \qquad (46)$$

Thus, the total range of $3\omega_1$ is 7π radians/display dimension, and the total range of $17\omega_2$ is 34.5π radians/display dimension, an acceptable preservation of the 5:1 ratio.

Figure 16 shows similar transform information for the same rectangle shifted so that its center is at (0,17) pixels. The magnitude plot is identical to the previous one, and the phase is identical in the ω_1 - direction, as expected, but displays a linear phase variation in the ω_2 - direction, produced by the shift in the y - coordinate.

Figure 17 shows the case for the rectangle centered at (17,0) pixels. Here, the ω_2 variation is the same as the original (Figure 15), as is the ω_1 magnitude variation. The ω_1 phase variation is linear, produced by the shift in the x - coordinate.

Figure 18 depicts the rectangle centered at (17,17) pixels. The magnitude variation is the same as for the original (Figure 15). The phase variation shows linear components in both ω_1 and ω_2 directions, and has become rather complicated, as noted previously for the 35 x 35 pixel square, similarly displaced.

It may be concluded that, given familiarity with the image function, the magnitude information will disclose what image is present. The phase information will allow determination of the location of the image within the field-of-view. Based on this generalization, a common strategy is to concentrate on the magnitude information and neglect the phase information, the

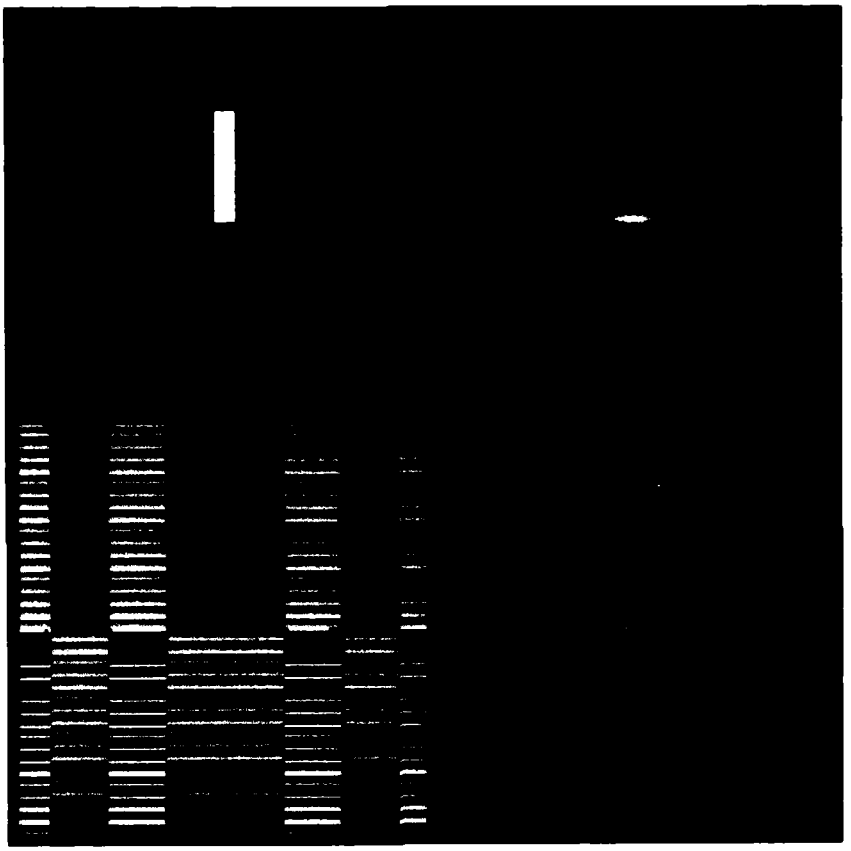

Figure 16. Pictorial Transform Study of a Rectangle, 7 x 35 Pixels, Centered at (0,17)

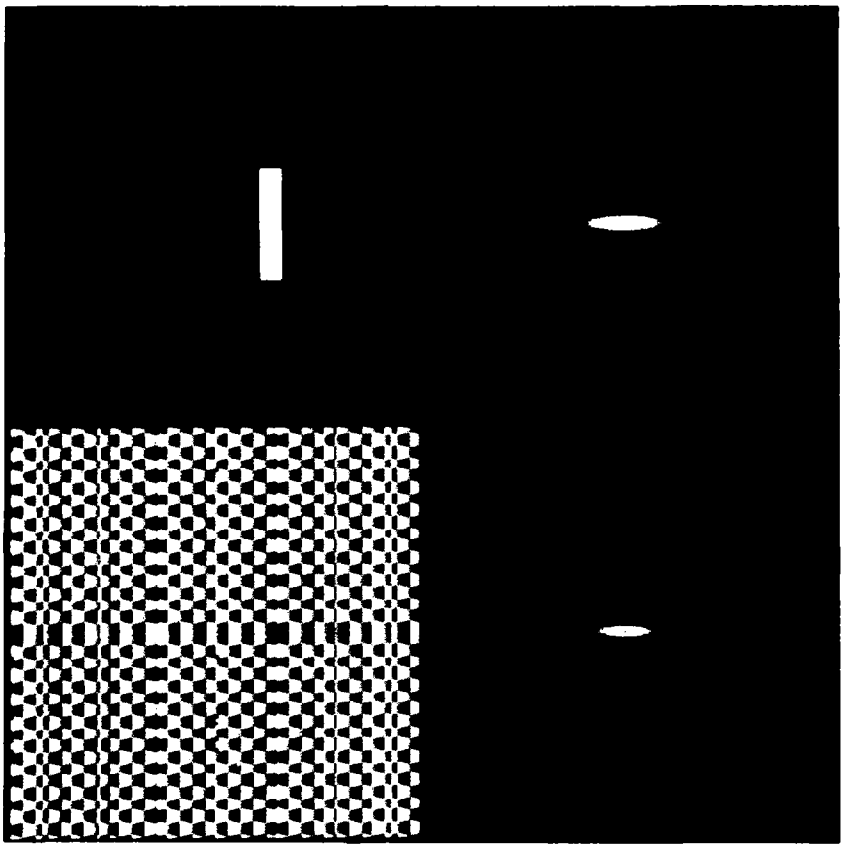

Figure 17. Pictorial Transform Study of a Rectangle, 7 x 35 Pixels, Centered at (17,0)

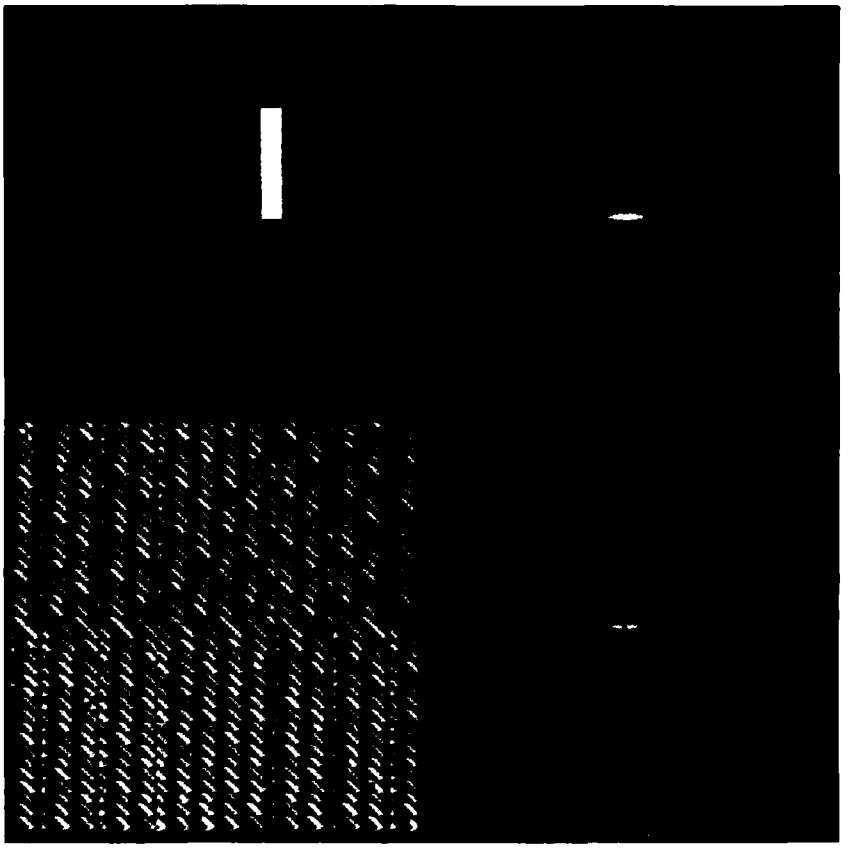

Figure 18. Pictorial Transform Study of a Rectangle, 7 x 35 Pixels, Centered at (17,17)

location within the field-of-view generally being obvious without resort to transform operations. This strategy is generally unwise, even though it is correct. In truth, the magnitude information and the phase information are not independent. Given one, the other can be determined (although perhaps with an unacceptable level of effort). Thus, the magnitude information contains data as to what, but not where, the object is. Orientation with respect to the field-of-view can be determined. The phase information contains data from which not only where, but also what image is present. It is neglected, therefore, at the experimenter's peril.

The analysis performed here seems to be rather simple, and relatively unproductive, in view of the quantity of data present. It is, nevertheless, typical of that which can be accomplished in the absence of other data. The crucial ingredient is the skill and familiarity of the experimenter with elemental image shapes and their transforms from which image processing gains can be realized. Here again, a mental synthesis, from the superposition of shapes present, of the transform magnitude function may be possible without undue difficulty. Not so, in general, for the phase. The comparison of data for an unknown image with a library of data for known images (map-matching or template-matching) can be rather more productive in those cases to which it is applicable.

Possibly the most general attitude that could be adopted, at least with respect to the simple images considered to this point, is that they consist of sample arrays of impulses such as those in Figures 5, 6, 7, and 8. For each of these functions, the magnitude function is unity, with the phase function varying according to position. The 7 x 35 pixel rectangle is composed of 245 such impulses, each with its own displacement from the center of the field-of-view. If only the magnitude functions were considered, one might expect the transform magnitude to be uniform over the ω_1 - ω_2 plane with a magnitude of 245. However, the interaction ("constructive interference," "destructive interference") pattern formed by the phase plots (possibly 35 varying only with ω_2; the other 203 varying with both) has the effect of not only producing a complex phase structure, but also producing the complex magnitude variation on the ω_1 - ω_2 plane. For more general images, not all brightness values are either one or zero, and a perceptual

decomposition in terms of an array of impulses becomes hopelessly complicated. This is, nevertheless, an accurate description of the physical process at work, as can be seen from the defining relationship in Equation (22), repeated here:

$$\mathcal{F}[f(x,y)] = A\ (\omega_1,\ \omega_2)\ \varepsilon^{j\theta(\omega_1)}\ \varepsilon^{j\phi(\omega_2)} \tag{47}$$

The modification in the magnitude function is produced by the sum of the phase functions:

$$\varepsilon\ j[\theta\ (\omega_1) + \phi\ (\omega_2)] \tag{48}$$

Analysis of this type has been accomplished in certain physical situations with some success. In the situation being addressed here, and with a field-of-view of 128 x 128 pixels, more than 16,000 impulse strengths and phase patterns could conceivably be involved. Thus, a decomposition on this basis would seem to be best accomplished over the entire array, using the 2DFFT. Other building-block concepts may be utilized by accepting degradations in resolution.

Section 5
IMAGE CONSTRUCTION USING SQUARES

It would seem to be obvious that, if the pixels in a 128 x 128 pixels field-of-view are too numerous for decomposition of the image by other than machine techniques, the alternatives are to increase the size of the elemental decomposition unit, or to decrease the number of pixels within the field-of-view. The approaches should, of course, produce comparable results.

A demonstration of a combination of these (increased elemental unit and reduced FOV) approaches has been accomplished, using the 35 x 35 pixel square of Figures 9, 10, 11, and 12 as the basic image, and considering it as, first, a 7 x 7 array of 5 x 5 pixel squares, and second, a 5 x 5 array of 7 x 7 pixel squares. These results are shown and discussed here.

Depicted in Figure 19 are the data for a single 5 x 5 pixel square within a 128 x 128 pixel FOV. As the image is smaller than those considered previously, one notes the slower variation with spatial frequency, and the visibility of off-axis lobes. With regard to the phase plate, a similar shaping is noted. With respect to the black areas within the white rectangles, it is noted that they denote the same phase values. The gray areas (no pun intended) are quite well defined.

Figure 20 is for a symmetric array of five 5 x 5 pixel squares within a 15 x 15 pixel square, and Figure 21 is for a symmetric array of four 5 x 5 pixel squares within a 15 x 15 pixel square. Because symmetry exists in the image, it is retained also in the transforms. Furthermore, the patterns associated with the single 5 x 5 pixel square are discernible, within which the "structure" caused by the symmetric "arraying" of identical figures can be attributed to a coherent interference phenomenon, the coherence originating in the transform operation, not the image. Figures 22 and 23 show 7 x 7 arrays of 5 x 5 pixel squares, again with symmetry retained in the images, and in the transforms. The basic patterns for the 5 x 5 pixel square are still present, but most observable, as one would anticipate, in the phase frames. Since the sum of the images is the 35 x 35 pixel square

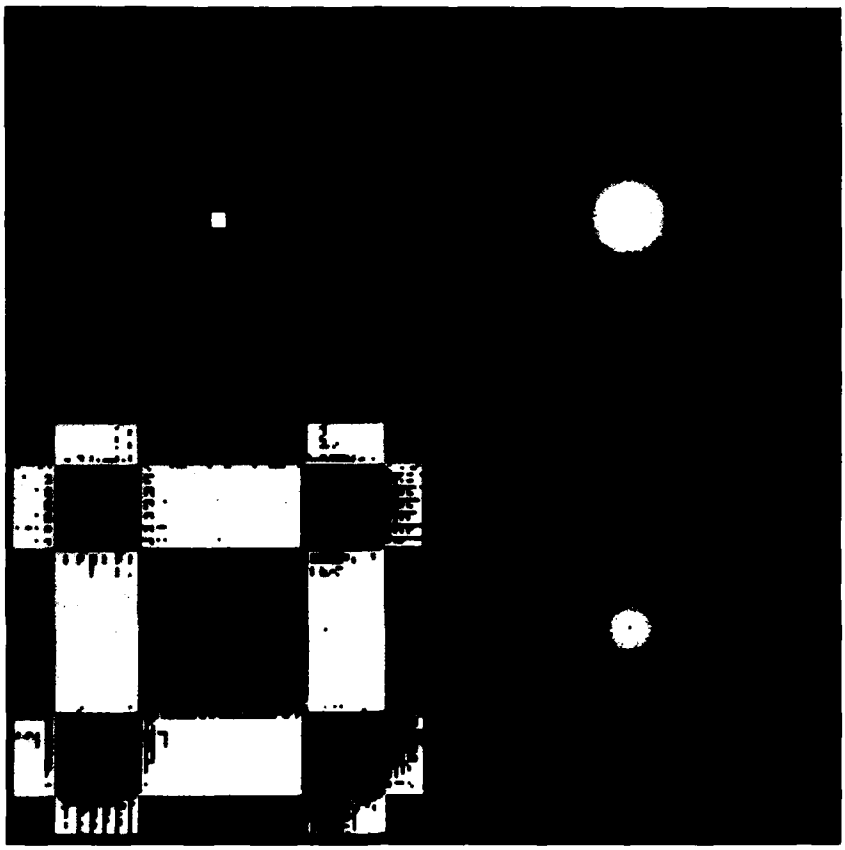

Figure 19. Pictorial Transform Study of a 5 x 5 Pixel Square, Centered at (0,0)

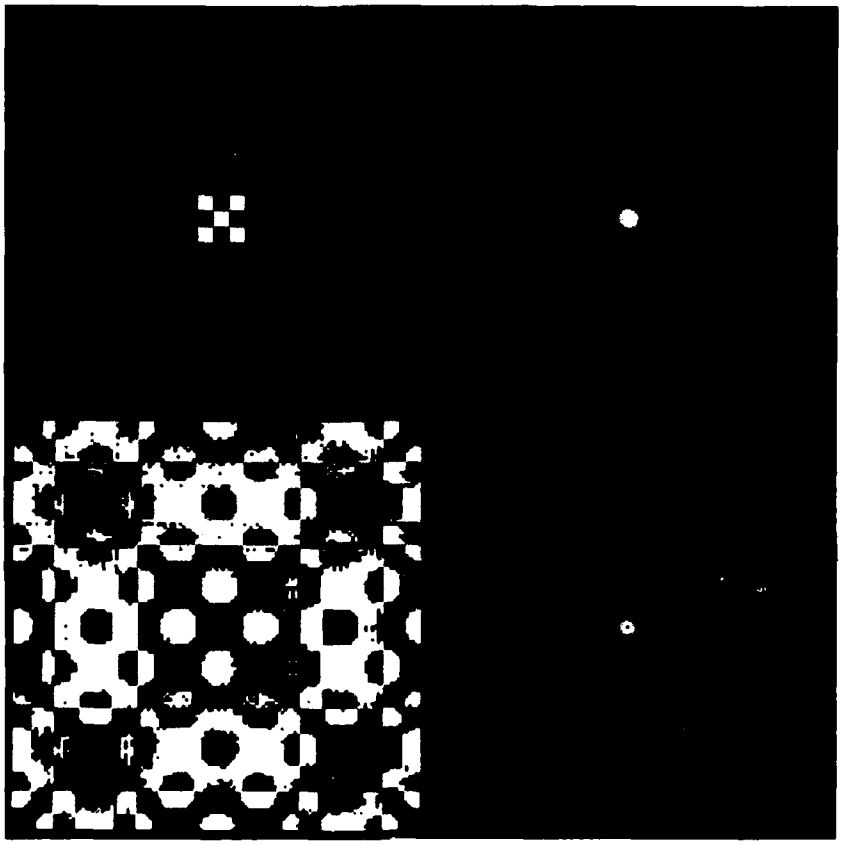

Figure 20. Pictorial Transform Study of a Symmetric Array of Five 5 x 5 Pixel Squares in a 15 x 15 Pixel Matrix, Centered at (0,0)

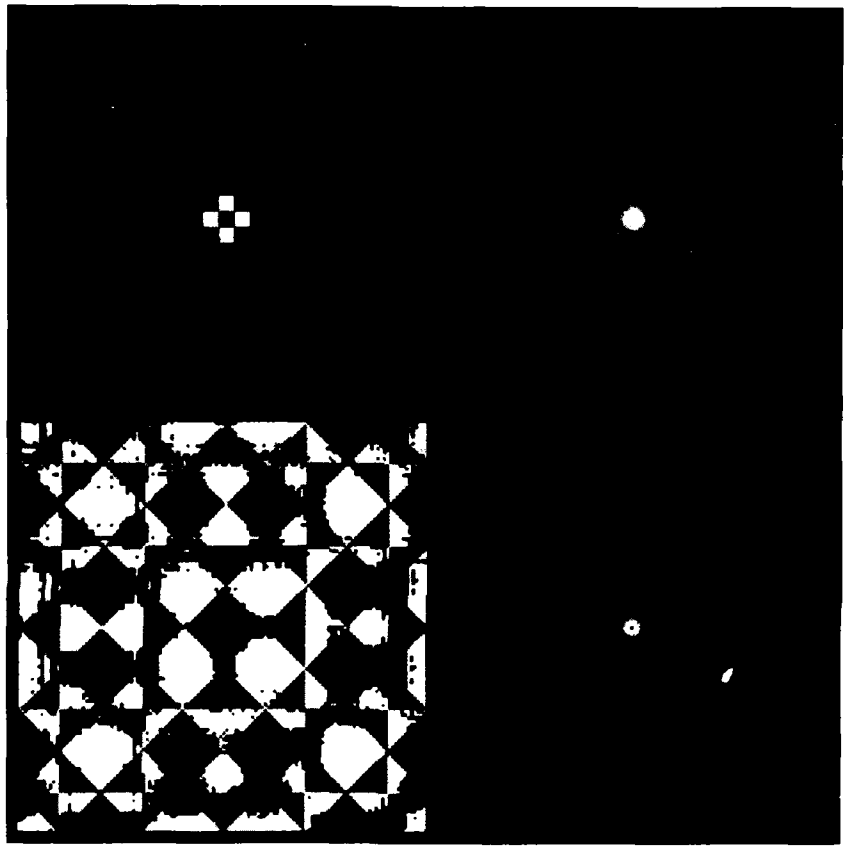

Figure 21. Pictorial Transform Study of a Symmetric Array of Four 5 x 5 Pixel Squares in a 15 x 15 Pixel Matrix, Centered at (0,0)

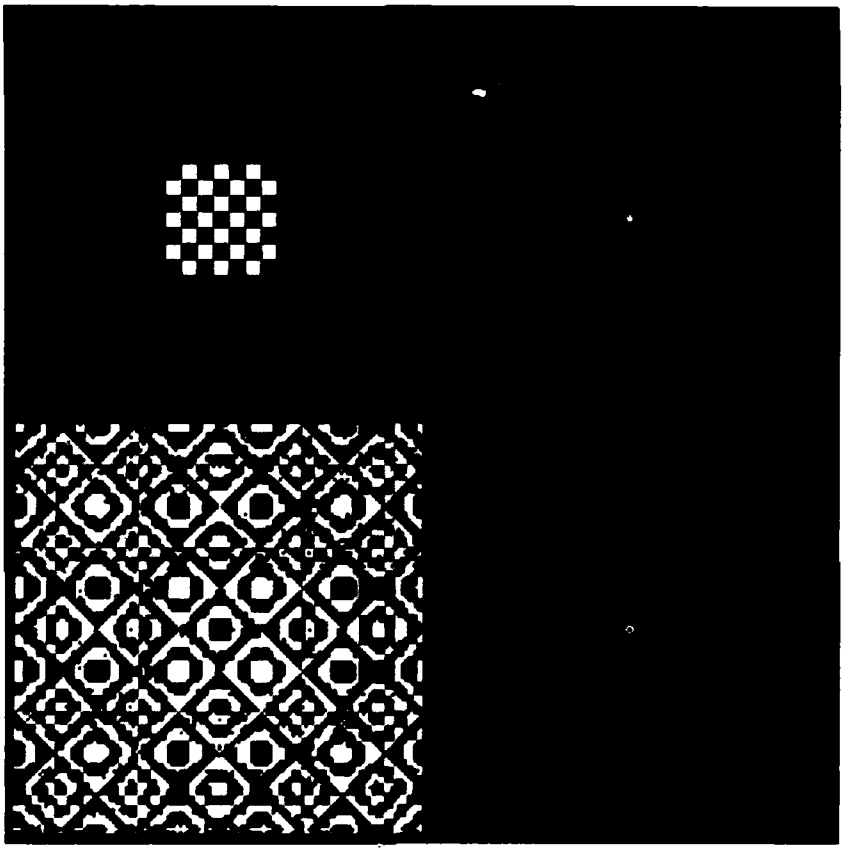

Figure 22. Pictorial Transform Study of a Symmetric Array of 24 5 x 5 Pixel Squares in a 35 x 35 Pixel Matrix, Centered at (0,0)

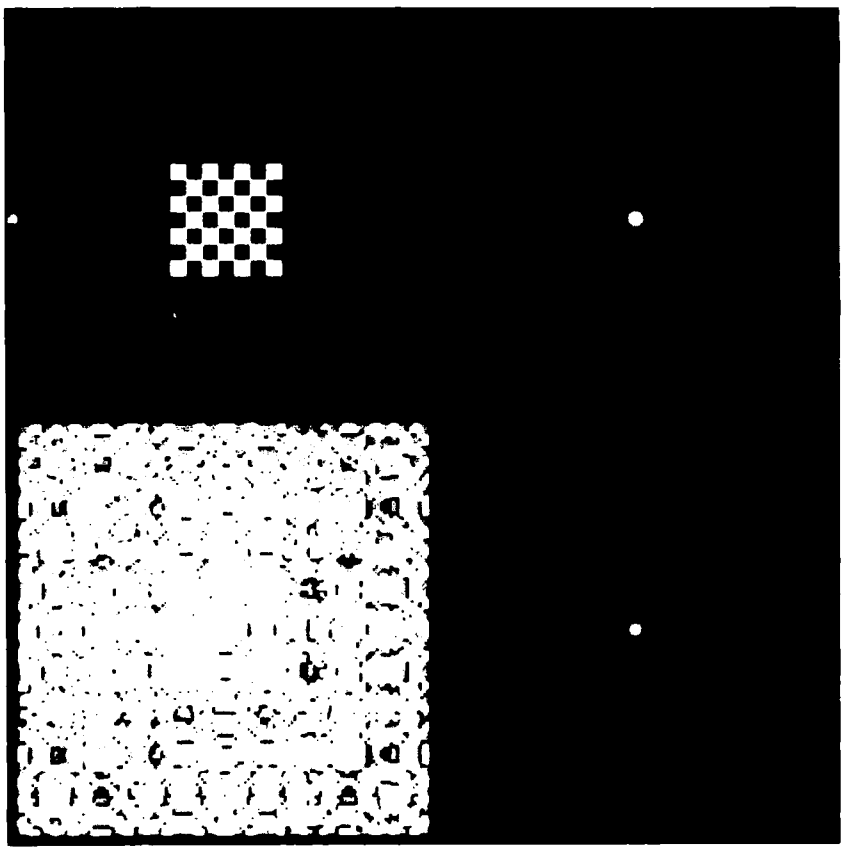

Figure 23. Pictoral Transform Study of a Symmetric Array of 25 5 x 5 Pixel Squares in a 35 x 35 Pixel Matrix, Centered at (0,0)

(Figure 9), the sum of the transforms is the transform of the 35 x 35 pixel square. In terms of Equation (47),

$$A_{35}\ (\omega_1,\omega_2)\ \varepsilon^{j\theta_{35}(\omega_1)}\ \varepsilon^{j\phi_{35}(\omega_2)} = A_{25}\ (\omega_1,\omega_2)\ \varepsilon^{j\theta_{25}(\omega_1)}\ \varepsilon^{j\phi_{25}(\omega_2)}$$

$$+ A_{24}\ (\omega_1,\omega_2)\ \varepsilon^{j\theta_{24}(\omega_1)}\ \varepsilon^{j\phi_{24}(\omega_2)} \qquad (49)$$

It is unfortunately true that

$$A_{35}\ (\omega_1,\omega_2) \neq A_{25}\ (\omega_1,\omega_2) + A_{24}\ (\omega_1,\omega_2) \qquad (50)$$

because of the coherence related to the transformation. During laboratory experimentation, the truth of Equation (49) has been carefully verified.

The coherence and symmetry properties noted here are completely predictable, and serve only to acquaint the reader with the significance of symmetry. This done, the effects of simple types of asymmetry are hopefully more clear.

For instance, in Figure 24, one white 5 x 5 pixel square has been removed from Figure 23, in a position that maintains symmetry with respect to the x-axis, but not the y-axis. The resulting amplitude plot is not remarkably altered, but the haze plot change is of significant interest. Vestiges of the phase frame for Figure 23 are clearly visible, overlying a linearly varying component along the ω_2-axis, for which the given image is asymmetric. (It must be remarked that the photographic renditions contained herein can hardly be considered as data, having been "processed," in all senses of that word, too many times since its origination; the reader is encouraged to give attention to the gross aspects presented since the detail could be misleading).

In Figure 25, two white 5 x 5 pixel squares have been removed from Figure 23, in positions that maintain symmetry with respect to the x-axis, but not the y-axis. In Figure 26, the two squares are removed along an axis rotated by 45 degrees and symmetrically with respect to the center of the

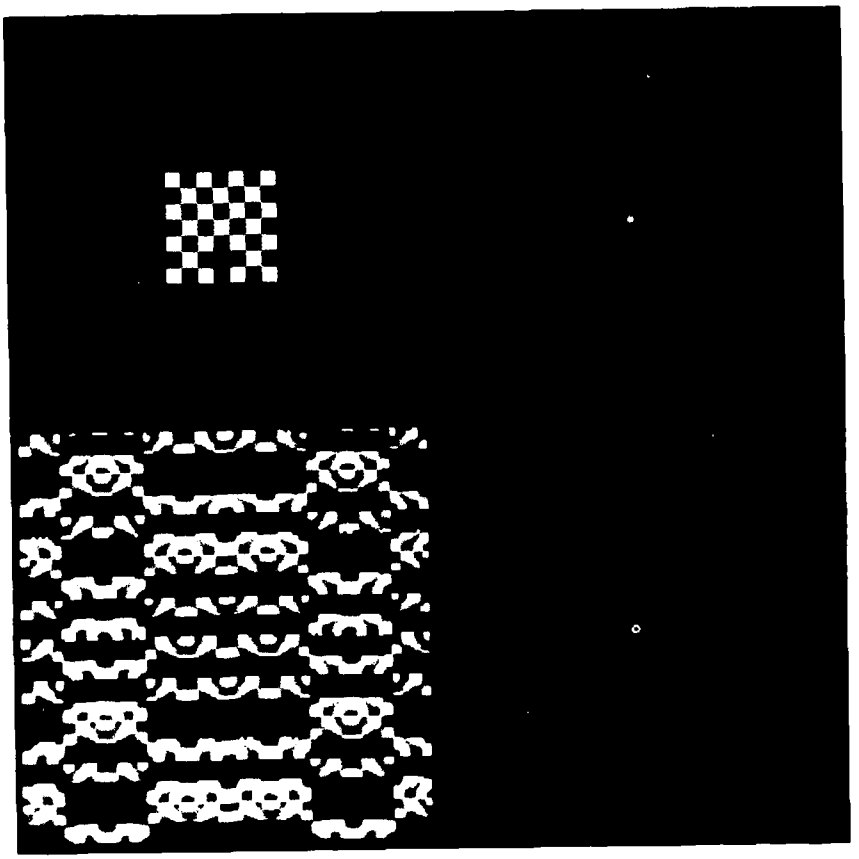

Figure 24. Pictorial Transform Study of an Asymmetric Array of 24 5 x 5 Pixel Squares in a 35 x 35 Pixel Matrix, Centered at (0,0)

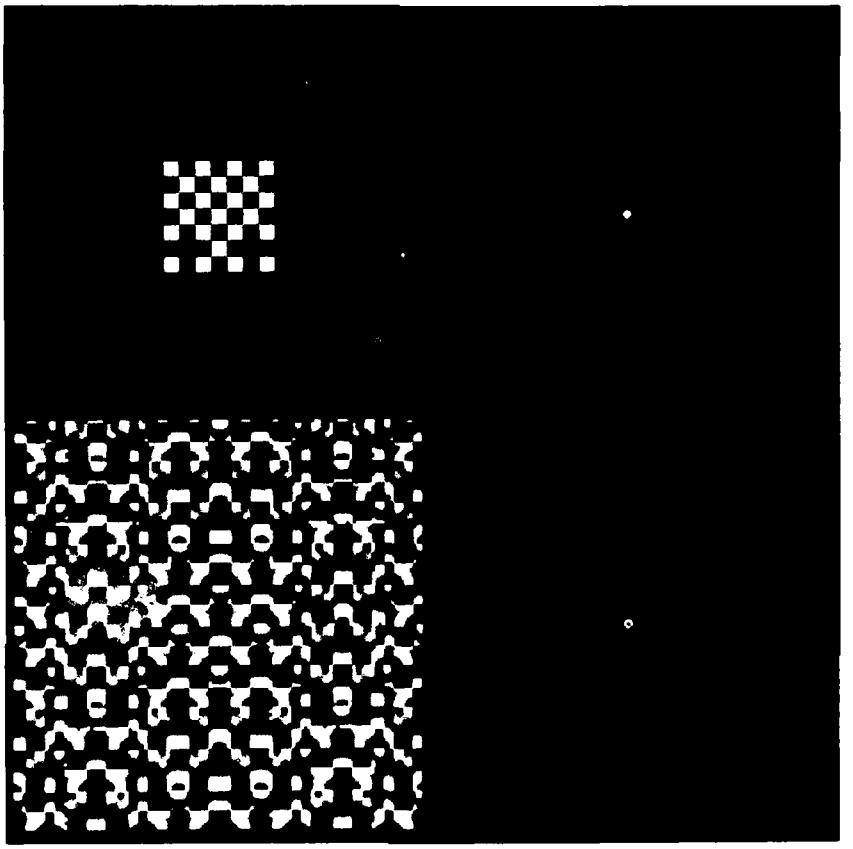

Figure 25. Pictorial Transform Study of an Asymmetric Array of 23 5 x 5 Pixel Squares in a 35 x 35 Pixel Matrix, Centered at (0,0)

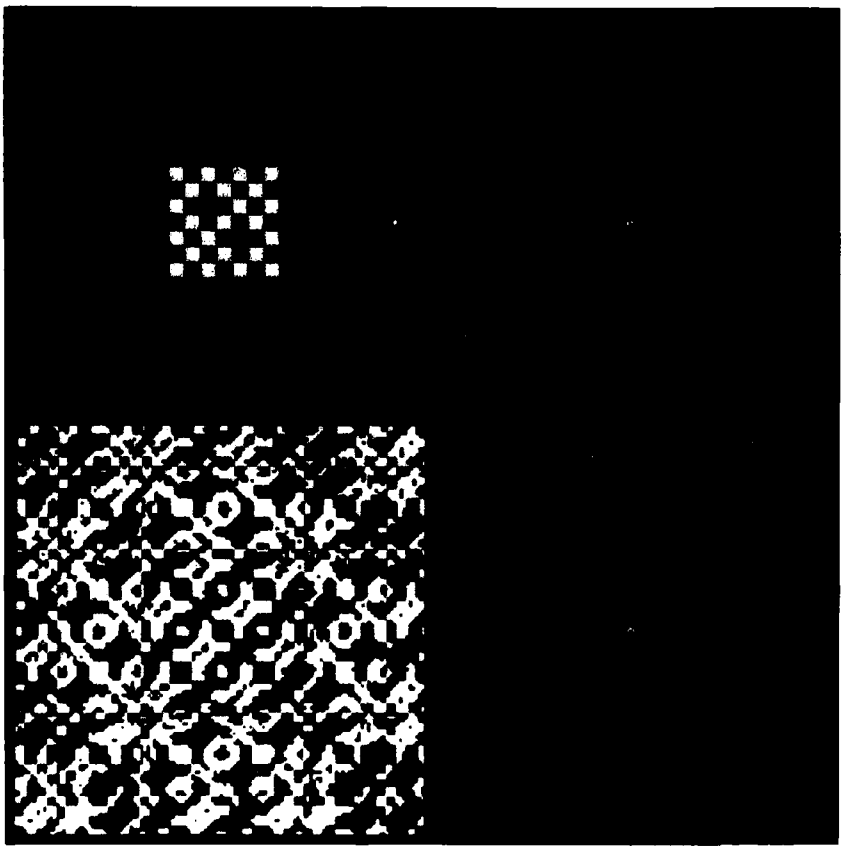

Figure 26. Pictorial Transform Study of an Asymmetric Array of 23 5 x 5 Pixel Squares in a 35 x 35 Pixel Matrix, Centered at (0,0)

square. Finally, in Figure 27, the two squares are removed along the rotated axis without symmetry with respect to the square's center.

The reader is urged to analyze these frames and draw conclusions concerning image decomposition, the relative information content of magnitude frames and phase frames, and the detectability of the original 5 x 5 pixel patterns in the transforms of the more complicated images.

Figures 28, 29, 30, 31, and 32 are similar to Figures 19, 20, 21, 22, and 23, except that the 5 x 5 pixel squares have been replaced by 7 x 7 pixel squares. The conclusions to be drawn are similar, and are attributable to a scaling factor on size, if that would be useful.

The "checkerboard" format used here is not without its own significance, and would be a viable choice in any conventional, fixed-orientation, raster-scanning system. It could undoubtedly be tied to a two-dimensional Walsh transformation, as well as the Fourier version, but with some loss of general appeal. Its use here, however, is motivated mainly by its compatibility with the more-or-less conventional raster scan, and by the arbitrary degree of complexity of the images which can be easily constructed electronically, and transformed. The word description analysis laid on the images and their transforms is indicative of the recommended approach for the experimenter not inclined to work out the mathematical expressions.

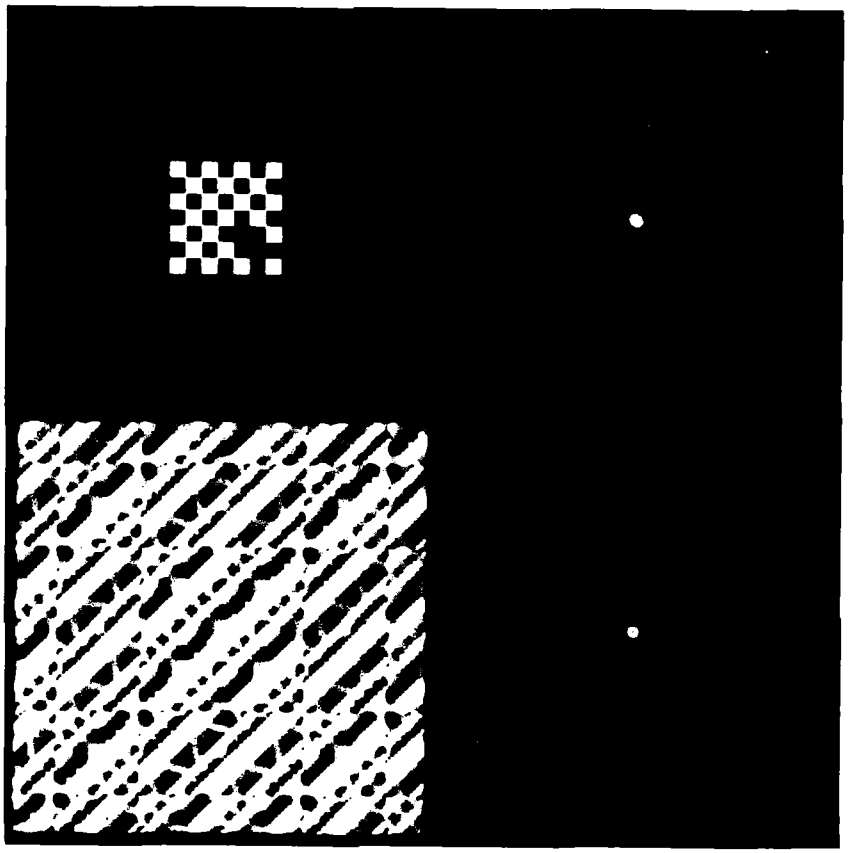

Figure 27. Pictorial Transform Study of an Asymmetric Array of 23 5 x 5 Pixel Squares in a 35 x 35 Pixel Matrix, Centered at (0,0)

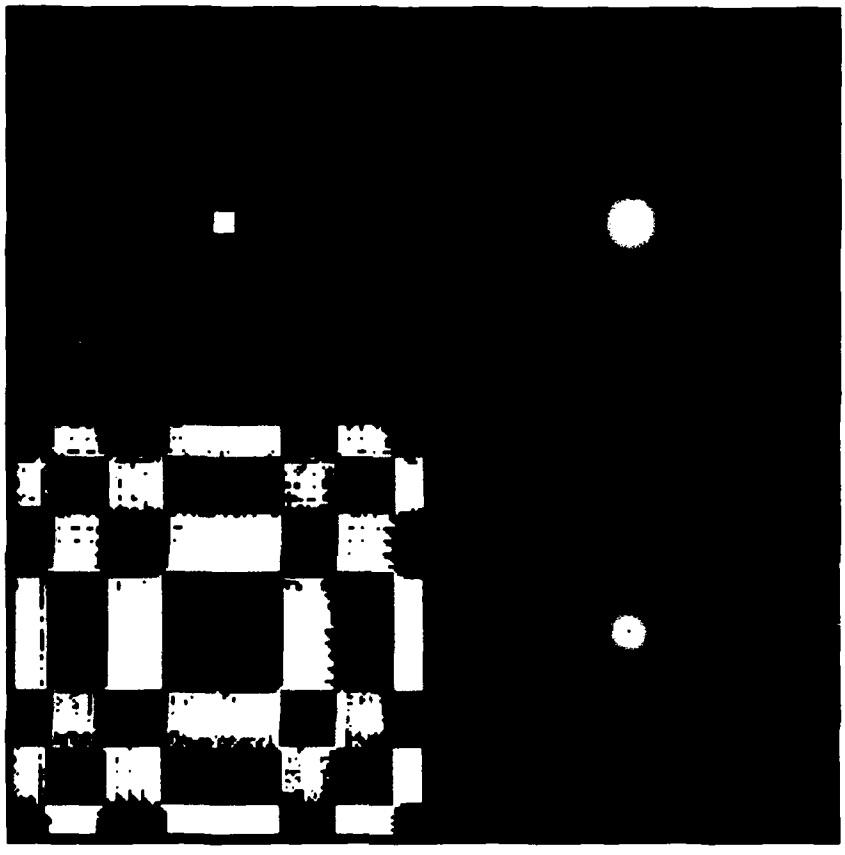

Figure 28. Pictorial Transform Study of a 7 x 7 Pixel Square, Centered at (0,0)

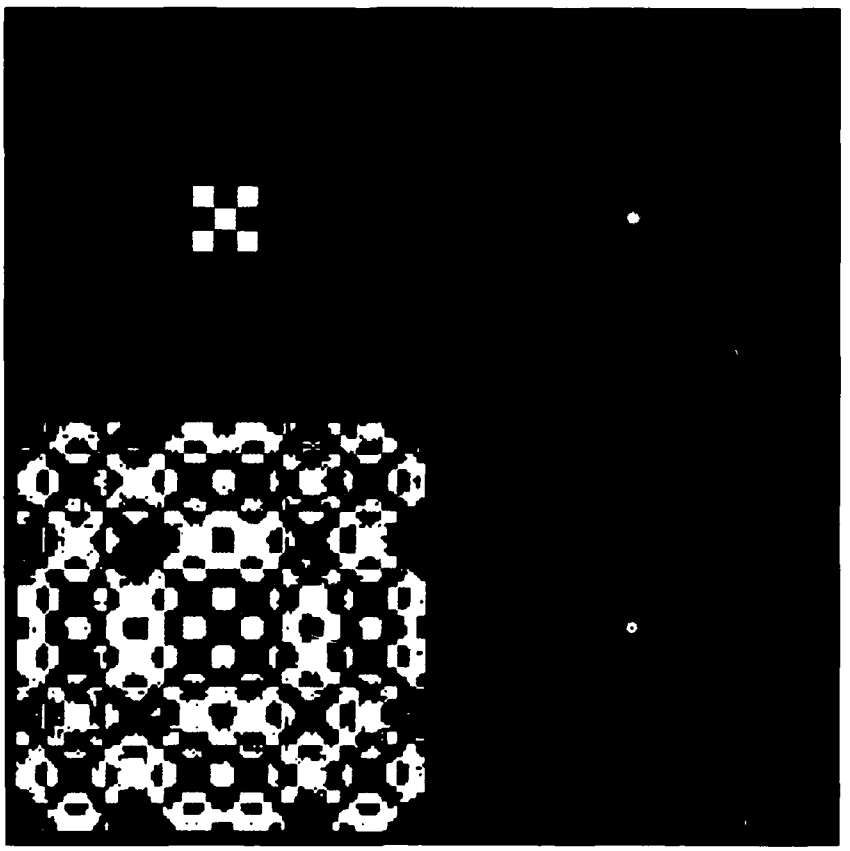

Figure 29. Pictorial Transform Study of a Symmetric Array of Five 7 x 7 Pixel Squares in a 21 x 21 Pixel Matrix, Centered at (0,0)

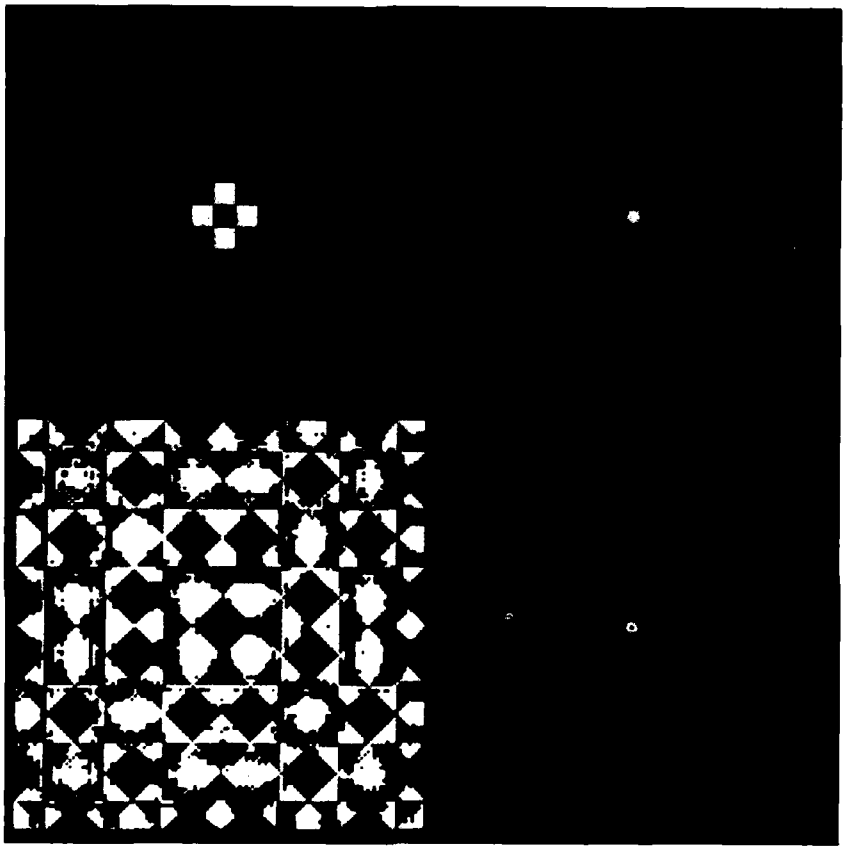

Figure 30. Pictorial Transform Study of a Symmetric Array of Four 7 x 7 Pixel Squares in a 21 x 21 Pixel Matrix, Centered at (0,0)

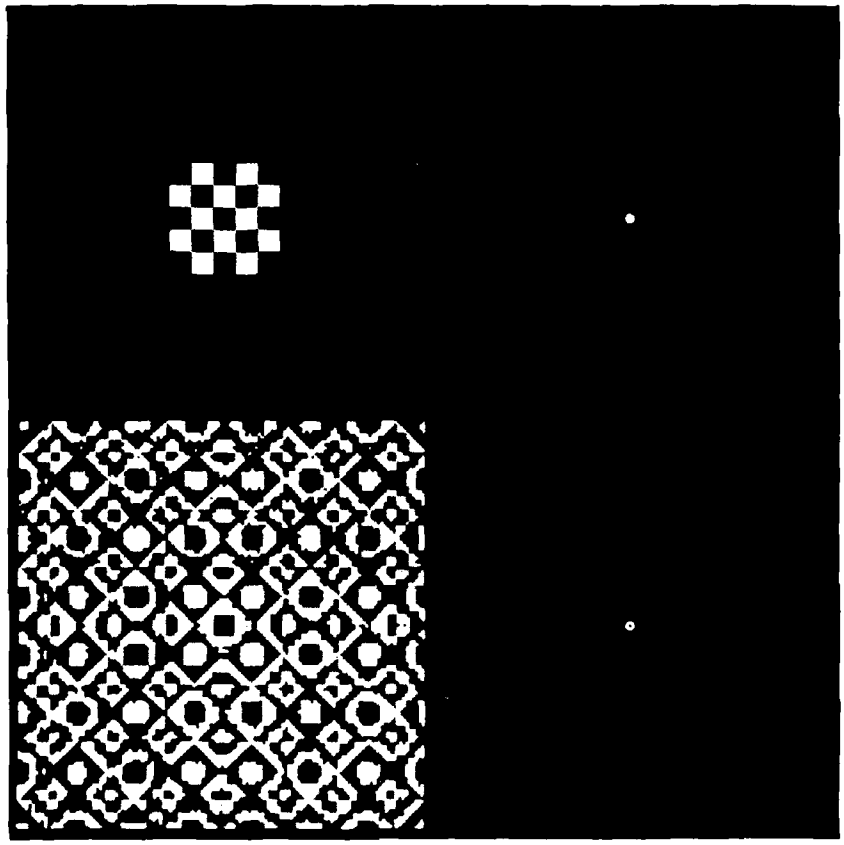

Figure 31. Pictorial Transform Study of a Symmetric Array of 12 7 x 7 Pixel Squares in a 35 x 35 Pixel Matrix, Centered at (0,0)

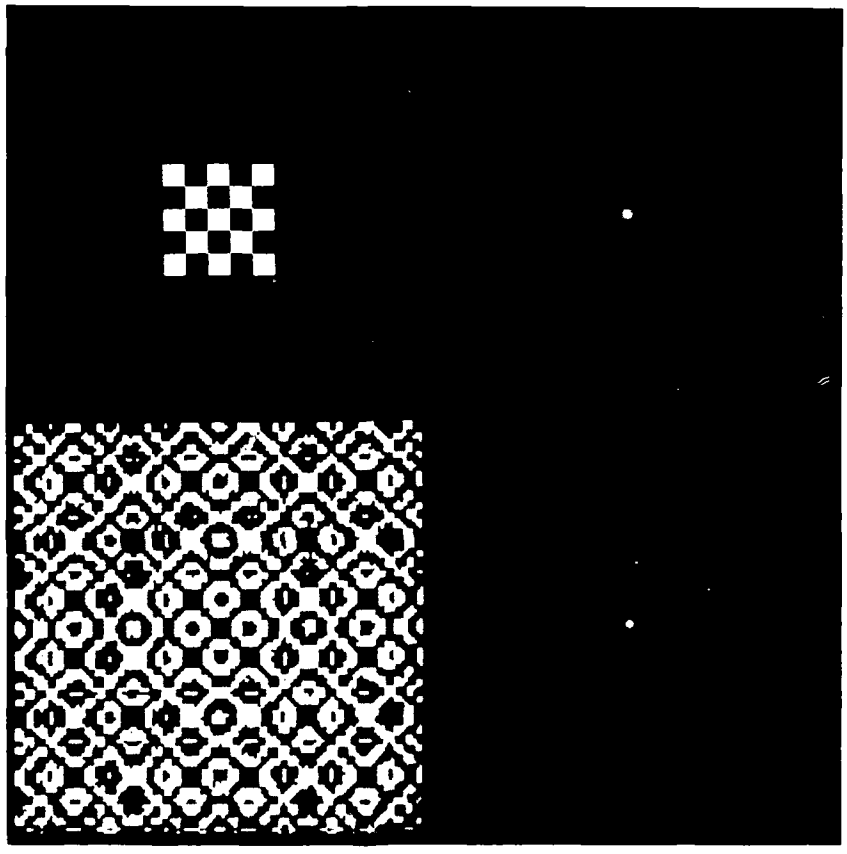

Figure 32. Pictorial Transform Study of a Symmetric Array of 13 7 x 7 Pixel Squares in a 35 x 35 Pixel Matrix, Centered at (0,0)

Section 6
MORE COMPLICATED IMAGES

The images discussed so far have one characteristic in common--they have been composed of areas within a 128 x 128 pixel field-of-view in which each pixel is either white or black. In the more normal case, the image would consist of various shades of gray, varying within the image area to constitute, in fact, the information contained in the image. Since it is appropriate to tie this situation to the images previously investigated, regular geometric shapes have been selected, and modeled with their bases in the plane of the image. Brightness, or gray shade, has been made to represent height above the base, with the highest points being white. This gradual increase in image complexity has been selected to acquaint the experimenter with the trends to be expected in the data obtained from more realistic images.

In Figure 33, a rectangular pyramid is presented, and the multiplicity of symmetry axes is evident in both the magnitude and phase frames. In Figure 34, a triangular solid is shown, and here the result of primary interest is the phase plot. In spite of the strong intensity variation along the x-axis in the image plane, phase variation occurs only along the ω_2-axis in the transform plane, similar to that for a rectangular shape of the base of the solid. Two conclusions can be drawn from this phase plot. They are:

1. The figure is centered in the field-of-view.
2. The triangular figure produced by the intersection of the solid and a plane normal to the y-axis produces no phase variation.

Thus, if this figure were displaced from center along the x-axis, a linear phase variation in the ω_1 direction would occur, similar to that observed earlier with the displaced impulses.

Figure 35 depicts a wedge-shaped solid and, because of its asymmetry, the linear phase variation mentioned above. In both figures, the ω_1 variation of magnitude correctly appears to be very smooth.

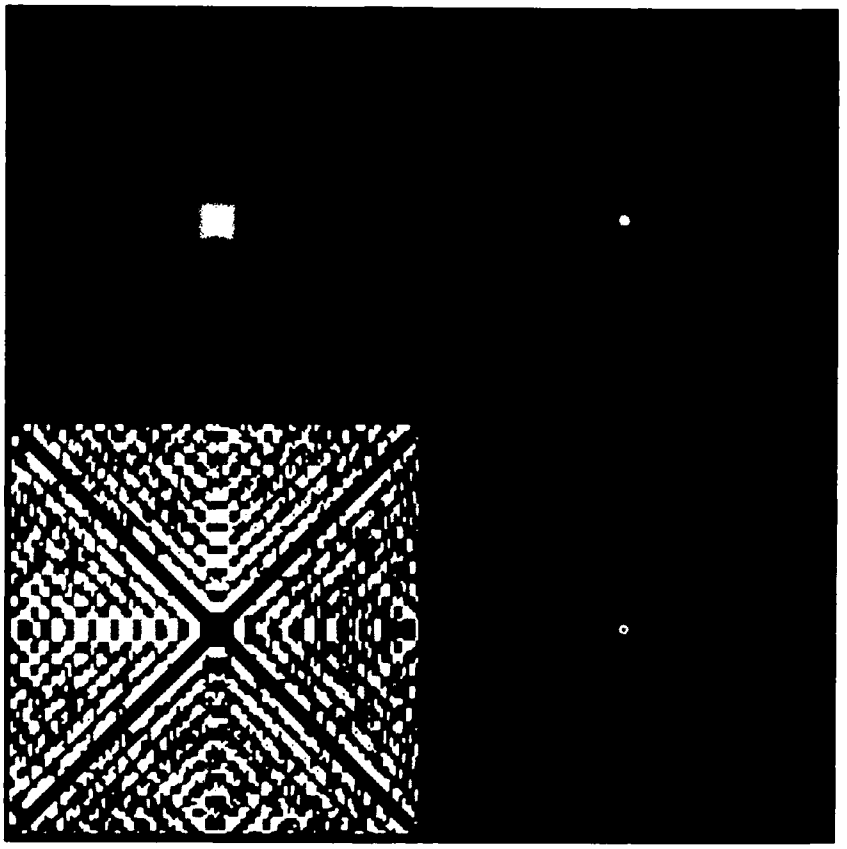

Figure 33. Pictorial Transform Study of a Rectanglar 35 x 35 Pixel Brightness Pyramid, Centered at (0,0)

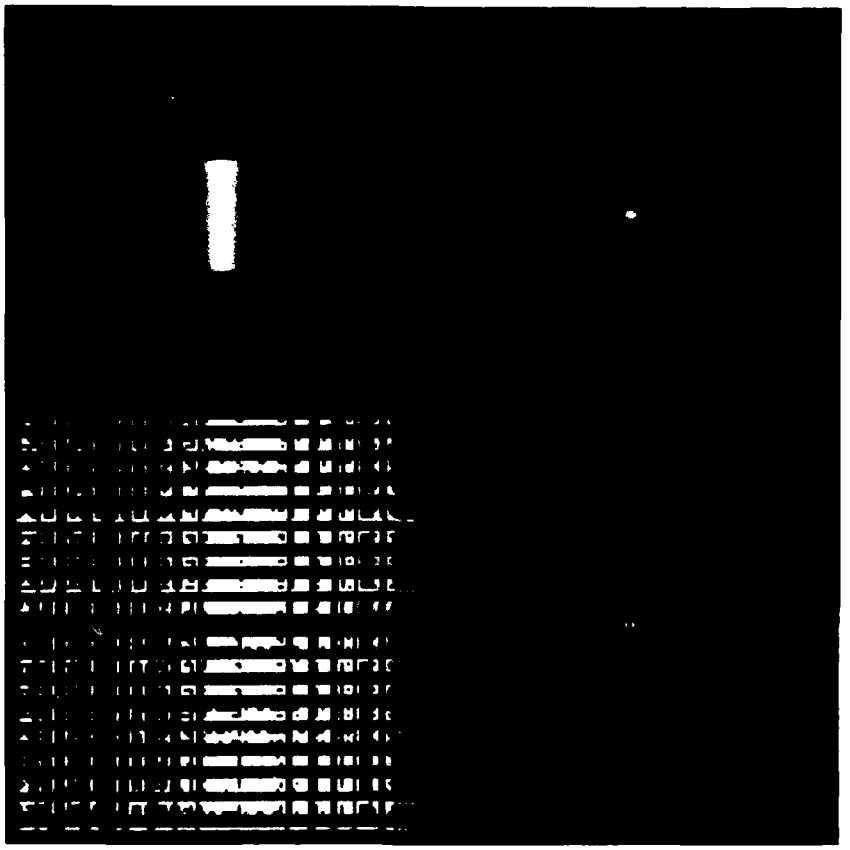

Figure 34. Pictorial Transform Study of a Rectangular 35 x 35 Pixel Brightness Triangle, Centered at (0,0)

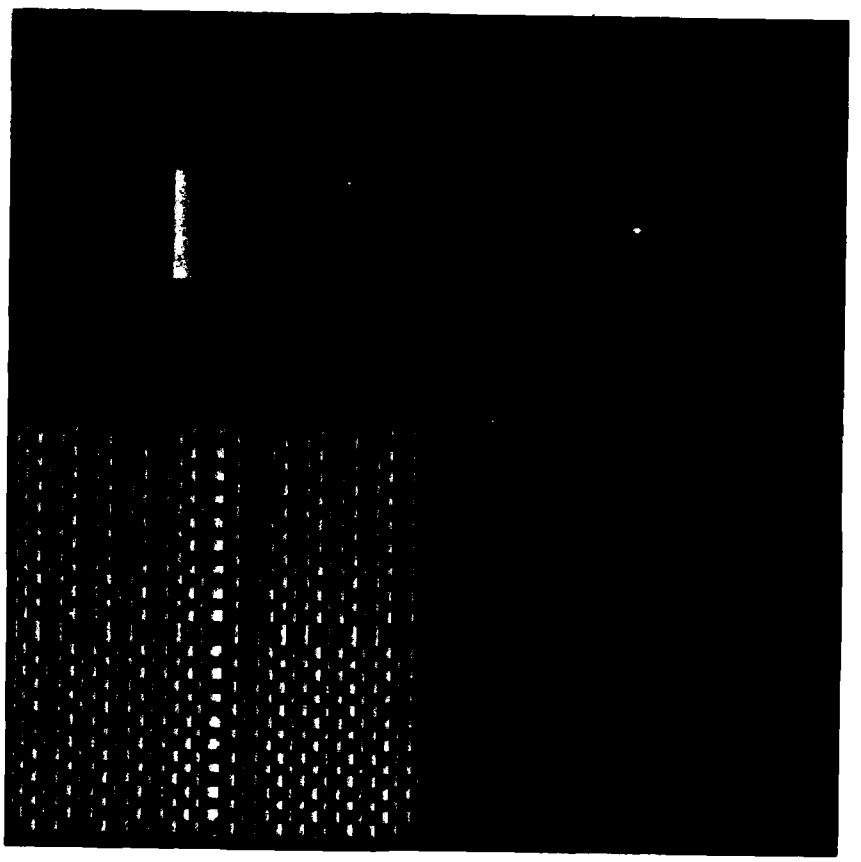

Figure 35. Pictorial Transform Study of a Rectangular 35 x 35 Pixel Brightness Wedge, Centered at (0,0)

Finally, in Figure 36, a cone-shaped solid is depicted. As noted before in the case of the circle (or cylinder, in the present context) circularly symmetric shapes are difficult to construct in a square format consisting of so few pixels. Thus, in the phase frame, the concentric ring structure is maintained for only three cycles. For higher spatial frequencies, the rectangular structure inherent in the raster scan format is evident, with eight symmetry axes apparent.

These phenomena are stressed because the experimenter must determine the best format in which to work, in consideration of the images to be investigated. In preliminary evaluations, the presence of artifacts of sampling must be determined, so that the number of pixels in the field-of-view may be set at the lowest value which produces acceptable resolution. As the number of pixels increases, so does the processing time and storage capacity required.

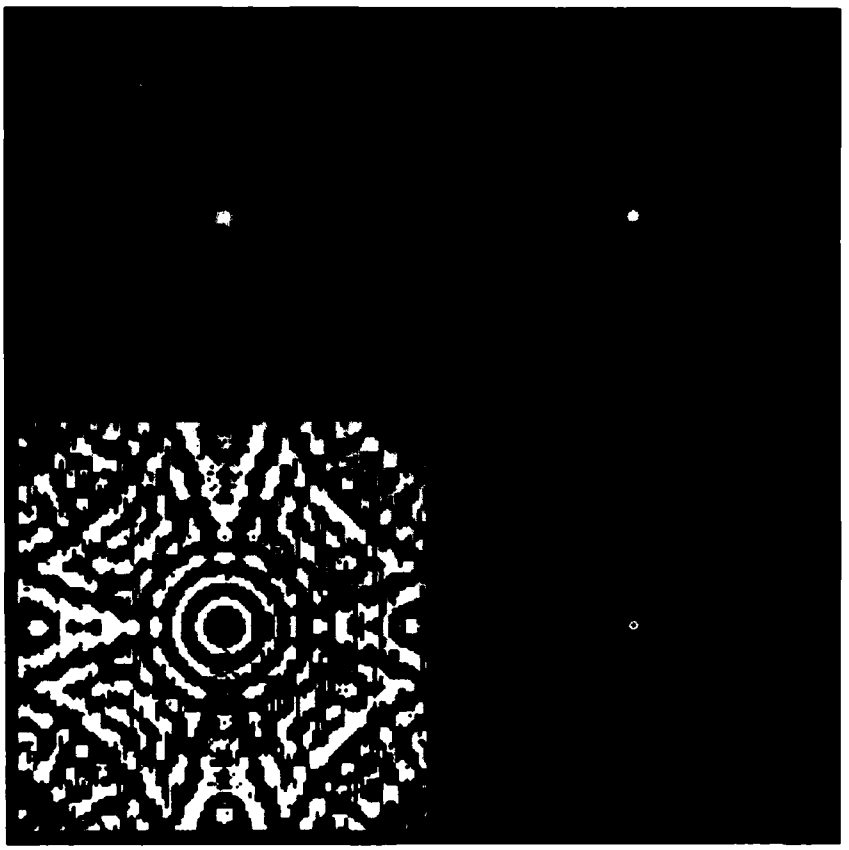

Figure 36. Pictorial Transform Study of a Circular Brightness Cone, Centered at (0,0)

Section 7
CONCLUSION

The purpose of this document is to serve as a tutorial for the experimenter preparing to use the VIPER facility for image processing using Fourier transform techniques. A considerable library of image transform data is presented for study by the experimenter, with the conviction that an understanding of the simple shapes presented will assist in the evaluation of more realistic images and transforms.

The facility staff can, of course, assist the new experimenter in understanding the limitations imposed by the apparatus from the input sensors to the various output formats. In general, however, the experimenter must recognize valid results, and be able to interpret their physical significance.

BIBLIOGRAPHY

Blackman and Tukey, 1959, "The Measurement of Power Spectra from the Point of View of Communication Engineering, Dover.

Bracewell, R. N., 1978, "The Fourier Transform and its Application," Second Edition, McGraw-Hill.

Dudgeon and Mersereau, 1984, "Multidimensional Digital Signal Processing," Prentice-Hall.

Gonzalez and Wintz, 1977, "Digital Image Processing," Addison-Wesley.

McGillem and Cooper, 1974, "Continuous and Discrete Signal and System Analysis," Holt, Rinehart and Winston.

Oppenheim and Schafer, 1975, "Digital Signal Processing," Prentice-Hall.

Papoulis, A., 1962, "The Fourier Integral and Its Applications," McGraw-Hill.

Stanley, W. D., 1975, "Digital Signal Processing," Reston.